Hydrogeology Journal (2023) 31:1331–1352
https://doi.org/10.1007/s10040-023-02642-5

REPORT

Montagne Pelée volcano (Martinique, in the French Lesser Antilles) hydrogeological system revealed by high-resolution helicopter-borne electromagnetic imagery

Benoit Vittecoq[1,2] · Pierre-Alexandre Reninger[3] · Vincent Bellier[1] · Anne-Lise Taïlamé[1] · Laureen Nacimento[1] · Emile Gros[1] · Sophie Violette[2,4]

Received: 10 October 2022 / Accepted: 9 May 2023 / Published online: 13 June 2023

Abstract
Montagne Pelée, on the French island of Martinique, eastern Caribbean Sea, has been one of the deadliest volcanoes in the world, with 30,000 victims following the 1902 eruption. Thousands of people still live nearby, and this volcano is a strategic "water tank" for Martinique Island, providing 40% of the island's water supply. This research aimed to better understand its hydrogeological functioning and the relationship with its complex volcanological evolution, taking advantage of a high-resolution helicopter-borne geophysical survey correlated with hydrogeological data from the boreholes and springs databases. Electromagnetic data, correlated with hydrogeological data, allowed for the identification of unsaturated zones, aquifers, and seawater intrusions, as well as the main geological units. In addition, data synthesised from pumping tests revealed that the older the unconsolidated pyroclastic deposits, the lower their hydraulic conductivity. The structural asymmetry between the northeastern and southwestern volcano flanks impacts its hydrogeological functioning. Consequently, the Montagne Pelée hydrogeological conceptual model is marked by several distinguishable aquifers. The upper perched aquifer within recent lava domes is directly involved in, and impacted by, phreatic eruptions, and it supports low flowrate springs. The remaining effective rainfall infiltrates to depth and recharges the hydrothermal system through vertical fractures. The other aquifers are categorized into three groups: northeastern, southeastern and southwestern flank aquifers. This research is a new step toward a better understanding of the Lesser Antilles volcanoes and more broadly of the central and proximal parts of the andesitic active volcanoes.

Keywords Volcanic aquifer · Electromagnetic geophysical methods · Conceptual model · Island hydrogeology · Martinique (France)

Introduction

Over 29 million people live on the flanks of active volcanoes (Brown et al. 2017). Among the essential needs of a population, access to water is crucial for both drinking purposes and irrigation, especially on volcanic islands. Furthermore, surface water and groundwater are often affected by volcanic activities or are involved in the eruptive processes—for example, groundwater plays a key role in phreatic eruptions (steam-driven explosions). Regarding all these concerns, it is necessary to gain a deep understanding of the geological structure and hydrogeological functioning of active volcanoes.

As shown by Cabrera and Custodio (2019), each island or each volcano has its own hydrogeological characteristics inherited from its geological history, structure and erosion processes. Nonetheless, they also share some characteristics. Thus, for each volcanic island, or for each active volcano, it is necessary to define adequate hydrogeological conceptual models at appropriate scales in order to allow an adaptive management strategy for water resources and to better constrain the interaction between volcanic activities and groundwater.

Historically, hydrogeological functioning of volcanic islands has been synthetized using two conceptual models,

✉ Benoit Vittecoq
b.vittecoq@brgm.fr

1 BRGM, 97200 Fort de France, Martinique

2 ENS-PSL Research University and CNRS, UMR.8538 – Laboratoire de Géologie, 24 rue Lhomond, 75231 Paris, France

3 BRGM, F-45060 Orléans, France

4 Sorbonne Universite, UFR.918, F75005, Paris, France

the Hawaiian model (Meinzer 1930; Peterson 1972; Macdonald et al. 1983); and the Canary Islands model (Custodio 1975; Custodio et al. 1988), both for basaltic islands. More recently, a conceptual model of old basaltic islands has also been proposed by Vittecoq et al. (2014), and a relationship between these models, with an evolution from recent Hawaiian type islands (<1 Ma) toward Canarian-type model islands due to weathering processes, has been proposed by Violette et al. (2014). None of these models are appropriate for describing the water resources of andesitic volcanoes.

Vessel and Davis (1981) and Bogie and Mackenzie (1998) have described the geological structure of andesitic volcanoes. Their conceptual model, based on the repartition of volcanoclastic deposits as a function of the distance to the event (central, proximal, median and distal) with heterogeneous facies (lava, pyroclastic deposits, tuff, tephra, air fall, breccia, debris avalanches, lahars and alluvial deposits), allows a better understanding of the hydrogeological functioning (Selles 2014; Selles et al. 2015). For the Lesser Antilles in the Caribbean Sea, Vittecoq et al. (2015), Hemmings et al. (2015) and Vittecoq et al. (2019) have described the hydrogeological functioning of central and proximal parts of mainly fissured and fractured andesitic lava aquifers dating from 1 to 15 Ma. Nevertheless, Lesser Antilles volcanoes are also characterized by young active pyroclastic edifices such as Soufriere Hills Volcano, Montserrat (Wadge et al. 2014), Soufriere, St Vincent (Robertson 1995; Pyle et al. 2018), Soufriere, Guadeloupe (Legendre 2012) and Montagne Pelée, Martinique (Westercamp and Traineau 1983; Westercamp et al. 1990; Michaud-Dubuy 2019).

Montagne Pelée is an iconic volcano, cradle of modern volcanology and one of the deadliest volcanoes of the world with more than 30,000 victims following the 1902–1905 eruption. This volcano is located in the north of Martinique Island (Fig. 1), an andesitic volcanic island of the Lesser Antilles volcanic arc, induced by the subduction zone between the Atlantic Plate and the Caribbean Plate (Westercamp et al. 1989). Thousands of people still live nearby and this volcano is a strategic "water tank" for Martinique Island. River intakes, springs and boreholes provide 40% of the water demands of the island (around 100,000 m^3/day). One of its particularities is the presence of porous and permeable pyroclastic deposits superimposed over several tens to hundreds of meters.

Helicopter-borne electromagnetic methods have demonstrated their applicability with respect to basaltic islands (d'Ozouville et al. 2008; Auken et al. 2009; Pryet 2011; Pryet et al. 2011, 2012), active volcanos (Dumont et al. 2019), and andesitic islands (Vittecoq et al. 2015, 2019), especially because of their ability to measure resistivity variations within the first few hundred meters of depth. Nevertheless, to the authors' knowledge, there has been no published research about pyroclastic volcanos and associated hydrogeological functioning. For Montagne Pelée, being an active volcano, the relationship with the hydrothermal system is also of interest and a better description of groundwater circulations should assist towards a better understanding of the eruptive processes.

This research takes advantage of a unique high-resolution helicopter-borne geophysical survey (Deparis et al. 2014) conducted over the Montagne Pelée (Fig. 2) correlated with geological and hydrogeological data from a database of boreholes and springs (Figs. 2 and 3) with the aim of deepening the comprehension of the structure and hydrogeological functioning of this active volcano and to define its hydrogeological conceptual model.

Study area

Geology

Located in the central part of the Lesser Antilles Archipelago (Fig. 1a), Martinique Island is a volcanic island particularly notorious for its active volcano, the Montagne Pelée. This volcano is particularly known for its series of violent, superficial and laterally directed explosions during the 1902–1905 dome-forming eruptions and especially the 1902 May 8th and August 30th events which killed about 30,000 people (Lacroix 1904).

Located in the northern part of the island (Fig. 1b), Montagne Pelée (1,397 m amsl) occupies an area of about 150 km^2. As described by Vincent et al. (1989), the Montagne Pelée is not a regular andesitic cone. Volcanic deposits are mainly found on its southwestern and northeastern flanks. To the southeast, Montagne Pelée products overlie the older Morne Jacob volcano (5.5–1.5 Ma, Germa et al. 2010). The history of the Montagne Pelée is a good example for demonstrating that eruptive-style changes occur during a volcano's lifetime within the same edifice. The first stage is marked by an effusive style with the dominant production of lava flows and domes, whereas the second and third stages are mainly explosive style, represented by pyroclastic products (Boudon and Balcone-Boissard 2021). The pyroclastic deposits of the Montagne Pelée mostly result from ash and pumice fallouts and diverse pyroclastic density currents (PDC, which are flows of hot gas, ashes and debris from the collapse of a lava dome or an eruptive column) produced during the successive dome-forming, subplinian and plinian eruptions.

Boudon and Balcone-Boissard (2021) have provided a new volcanic activity evolution description of the Montagne Pelée, defined in three stages (Fig. 3). The first stage, from 550–127 ka, is called the primitive Montagne Pelée. The dominant geological facies are andesitic lava flows and lava domes. This primitive volcano activity stopped at 127 ka (Germa et al. 2011a) following a supposed huge flank collapse (The Prêcheur event: 25 km^3) that partly destroyed the southwestern flank of the volcano (Vincent et al. 1989; Le

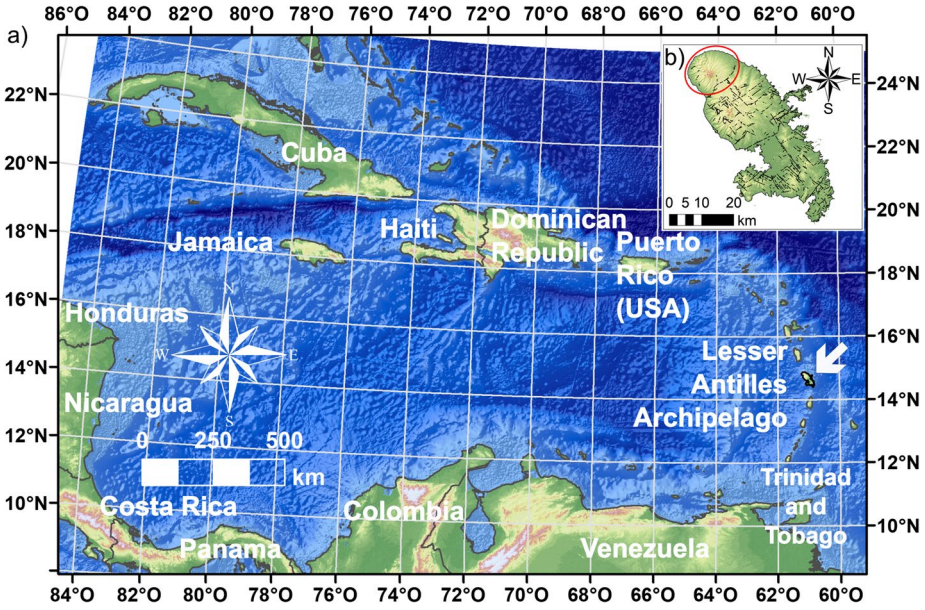

Fig. 1 **a** Location of the Lesser Antilles Archipelago and of Martinique Island (see arrow) and **b** location of Montagne Pelée on Martinique Island

Friant et al. 2003). The remains of this volcanic edifice are observable in the northwestern flank and described as the Mont Conil geological unit in previous studies (Westercamp et al. 1989). From 127 to 36 ka, during the second stage, the dominant volcanic activity was andesitic lava dome-forming and consolidated pyroclastic deposits. The third stage (36 ka to present day) is divided in two parts and begins following a supposed flank collapse (36 ka: The Rivière Sèche event, 1.8 km^3). The first part (36–25 ka) is dominated by numerous explosive eruptive events, mainly low silica subplinian and plinian deposits, filling the horseshoe-shaped structure induced by the flank collapse and then covering all the flanks of the volcano. The second part (25 ka to the present) diverges from the last one with an increase of silica content leading to volcanic products with an andesitic composition. The deposits result from alternating felsic plinian and subplinian events on one hand and dome-forming eruptions (recent lava domes and PDCs) on the other. Recently, Villemant et al. 2022 consider that the existence of two flank collapses ("Saint Pierre" and "Rivière Sèche"; Le Friant et al. 2003, Germa et al. 2011b) is questionable, as they are not recorded in their offshore cores. Pictures of geological outcrops of each stage are shown in Figures SI_1 and SI_2 in the electronic supplementary material (ESM).

Fumaroles, warm springs, and the hydrothermal system

Fumaroles activity, summarized by Barat (1986), was observed as being associated with the 1792 and 1851 phreatic eruptions. After each crisis, fumaroles activity rapidly decreases. In 1889, fumaroles restarted at the summit until the 1902 eruptions. Between 1903 and 1929 fumaroles activity did not stop and increased in 1929 before the eruption. After the 1929 eruption, the temperature of the fumaroles was 350 °C. Temperature rapidly decreased to stabilize at 100 °C, with chemical composition almost exclusively composed of CO_2. Then the fumaroles temperature continued to decrease until 1970 with the disappearance of the fumaroles of the Montagne Pelée. The last analysis (Fabre and Chaigneau 1960) showed a temperature of 80 °C and chemical composition close to the air (79% N_2, 20% O_2 and 0.5% CO_2).

The scarcity of thermal manifestations on the Montagne Pelée is supposed to be the result of permeable aquifers masking ascending fluids (Traineau et al. 1989). Seven groups of warm or thermal springs are observable on the flanks of the Montagne Pelée (Figs. 2 and 3): (1) the Chaude River springs (which appeared after the 1902 eruption according to Lacroix 1904) with current temperatures (recorded in 2022) between 24 and 32 °C (temperature declining over the past 50 years: 60–80 °C in the 1960s, 40–50 °C in the 1990s and the 2000s, and since then lower than 36 °C); (2) the Claire River springs (known before the 1792 phreatic eruption) with temperatures between 25 and 30 °C; (3) the Mitan-Picodo springs (also known before 1792), with temperature between 25 and 36 °C; (4) the Blanche River underwater springs (30–31 °C); (5) an underwater gas bubble emission zone between 2 and 8 m depth associated with several diffuse thermal water springs with temperature around 30 °C, located 1.5 km south from the Blanche River underwater springs; (6) the Grand Rivière spring, at an elevation of 865 m with 27 °C; and (7) the Des Pères River springs (20–23 °C). A small spring would also have been observed in the Prêcheur River but no more precise information is available. Finally, only one borehole has encountered thermal water, a 10-m-deep well

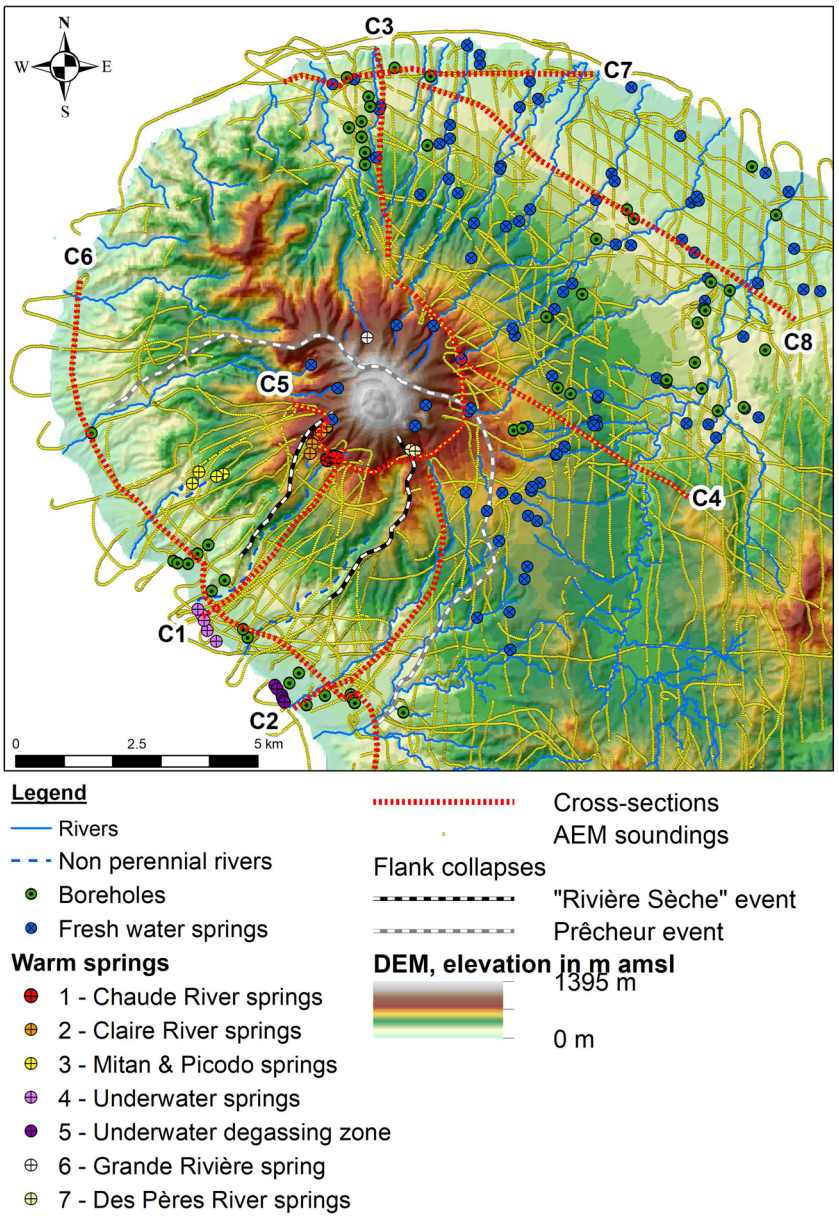

Fig. 2 Locations of flight lines, boreholes, freshwater springs, warm springs and rivers on the digital elevation model (DEM). Red lines correspond to the cross-sections (C1–C8) mentioned in section "Resistivity ranges of pyroclastic aquifers and the main geological units"

approximatively located 100 m upstream of the Blanche River underwater springs, with groundwater temperature around 30–32 °C and a mean water electrical conductivity of 1,267 µS/cm, monitored by the volcanic and seismic observatory of Martinique (Fontaine et al. 2022).

Traineau et al. (1989), then Gadalia et al. (2014), proposed several insights of the hydrothermal system functioning. The heat source, estimated around 800–900 °C, could be a magma chamber located at 5–8 km depth beneath the summit. At least two geochemical zones of the hydrothermal reservoir have been discerned. The first, feeding the Rivière Chaude springs, has bicarbonate-sodium composition (HCO_3–Na). The equilibrium temperature at depth, according to geothermometers (Na–K–Ca, Sr–K, Na–Li and Ca–K, Gadalia et al. 2014), would be between 180 and 200 °C. The second, supplying the Mitan and the Picodo springs, has sodium bicarbonate-chlorinated composition (HCO_3–Cl–Na), with a temperature of 155–180 °C at depth. The Blanche River underwater springs are expected to be the outlets of a lateral flow from the Chaude River springs through pyroclastic deposits (Traineau et al. 1989; Zlotnicki et al. 1998). Based on seismic monitoring, the hydrothermal system is supposed to be between 1 km above the sea level and 3 km below sea level (Boudon and Balcone-Boissard 2021).

Climate and surface hydrology

The Montagne Pelée climate is a typical humid tropical climate exposed to trade winds, with a rainfall rate increasing with elevation and heavier rainfall on the east flank because

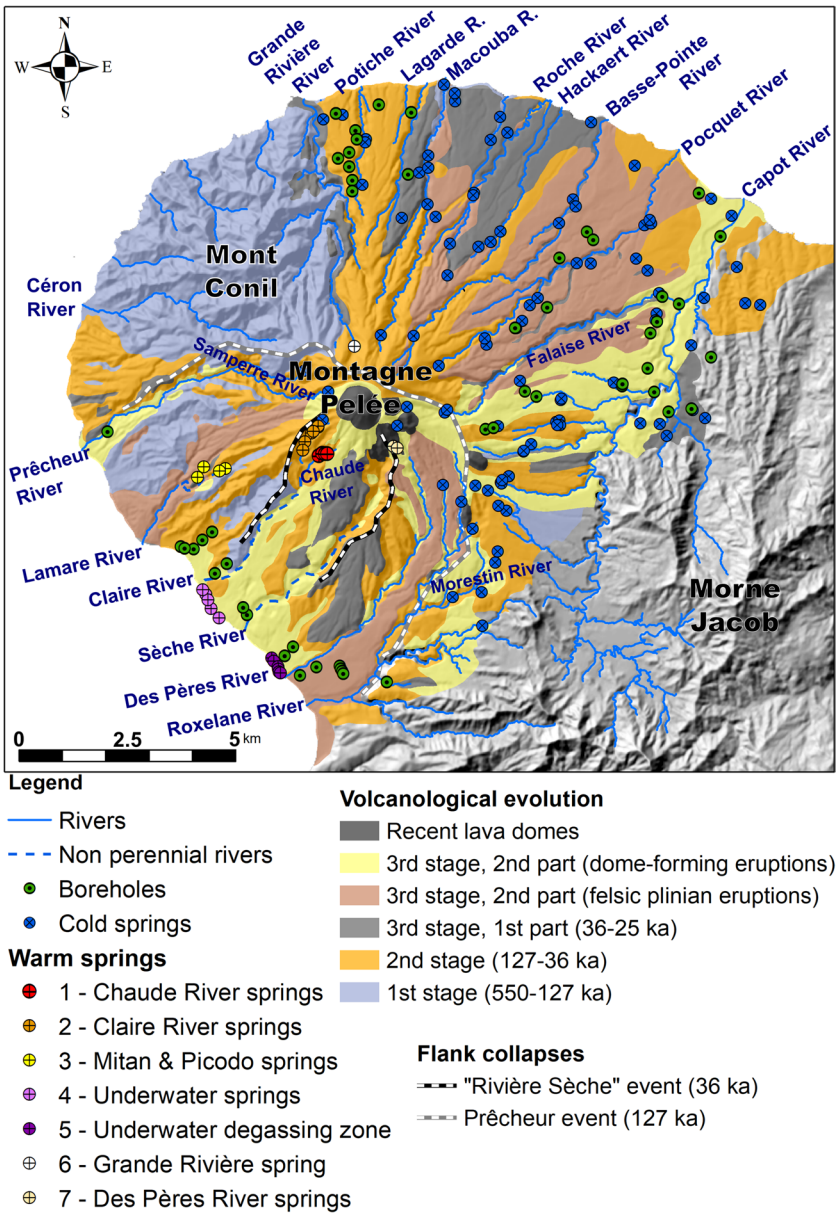

Fig. 3 Locations of boreholes, freshwater springs, warm springs and rivers on the geological map (Westercamp et al. 1990) modified thanks to the new volcanological evolution description by Boudon and Balcone-Boissard 2021

of the orographic effects of the volcano. Average annual precipitation (Fig. 4a) ranges from 2,000 mm at sea level on the west coast and reaching 4,600–6,900 mm at the summit (Guiscafre et al. 1976; Vittecoq et al. 2010).

Around 20 rivers flow on the Montagne Pelée volcano flanks. Their specific low water flowrate ranges between 18 and 35 L/s/km^2 with a median value of 23 L/s/km^2 (min 10 L/s/km^2 and max 60 L/s/km^2), the median value being similar on the two flanks. On the southwestern flank the notable difference is that the two rivers, the Sèche River and the Claire River, are mostly dry. The specificity of the Claire River is to be perennial in its upper part, between 800 and 480 m above mean sea level (amsl) elevation, and it fully infiltrates the pyroclastic deposits in an almost endorheic depression at 480 m amsl.

The large amounts of effective rainfall and the low river flows suggest that the amount of groundwater resource may be significant and should be stored in the pyroclastic deposits over thicknesses of a few tens to hundreds of meters. Nevertheless, knowledge regarding the extension and thickness of these deposits is not sufficiently detailed at the volcano scale. Furthermore, the complex geological evolution of the volcano and the impact of its asymmetry between the northeastern and southwestern flanks on groundwater circulation need to be characterized. These pyroclastic deposits also have interstitial porosity and unconfined aquifers, whereas aquifers over the rest of Martinique are mainly confined within fissured and fractured volcanic rocks (Vittecoq et al. 2015, 2019).

Thus, there is a necessity to more deeply characterize the hydrodynamic characteristics of the pyroclastic deposits and the interaction between rivers and groundwater. Given that the Montagne Pelée is an active volcano with a hydrothermal system at depth, a better understanding of the hydrogeological functioning is welcome to better understand the role of groundwater in the eruptive processes. There is then a clear interest to describe a hydrogeological conceptual model at the volcano scale.

Materials and methods

The methodology is based on coupling resistivity data from the heliborne electromagnetic survey conducted over the volcano in March 2013 (Fig. 2) with hydrogeological and geological field data and observations, especially thanks to 58 boreholes and 119 springs located on the volcano flanks, and to an existing hydrological water budget model.

Borehole and spring databases

A database of the 58 boreholes (Appendix 1) located on the volcano flanks has been assembled thanks to the BRGM archives collected since the 1960s. The database contains the main hydrogeological and geological available data: location, elevation, borehole depth, water level, aquifer geology, transmissivity, and hydraulic conductivity). Geological drilling descriptions were harmonized in order to take into account the most recent geological knowledge (Boudon and Balcone-Boissard 2021). Within this database, transmissivity data are available for 21 boreholes.

The springs database (Appendix 2 and Appendix 3) contains 119 springs, compiled from field reconnaissance carried out between 2005 and 2021. The database contains location and spring elevations. Freshwater springs (96, Appendix 2) and thermal springs (23, Appendix 3) are also discerned. This inventory could not be exhaustive but is nevertheless representative of the main springs and of the different hydrogeological contexts.

Helicopter-borne time-domain electromagnetic method

Martinique Island was covered by airborne electromagnetics (AEM) from February to March 2013 to address geological and hydrogeological purposes (Fig. 2). This survey, supervised by BRGM (French Geological Survey) and presented in Deparis et al. (2014), represented 4,233 line-kilometers for the whole island. The SkyTEM 304 system was chosen to image the shallow subsurface of this volcanic island (Sørensen and Auken 2004). Developed by the HydroGeophysics Group of the University of Aarhus (Denmark), this system operates in dual transmitter mode. The low moment (2,826 A.m^2: gates from 11 µs to 1 ms) provides information on the very near surface (the first 50–100 m), while the high moment (144.440 A.m^2: gates from ~70 µs to 8.9 ms) gives deeper information (~200 m).

The survey was mainly carried out along the N–S direction with a 400-m spacing and along the W–E direction with a 4,000-m line spacing; the spacing was locally refined to 200 m over areas of interest such as the Montagne Pelée. Along each flight line, AEM data were acquired every ~30 m, with an average ground clearance of 64 m due to the sharp topography of the island. Figure 3 (and Figure SI_3 in the ESM) shows the locations of the data over the studied area.

The AEM method allows one to image the conductivity/resistivity contrasts of the subsurface (Ward and Hohmann 1988). Its depth of investigation (DOI), around 200 m for this research, depends on the emitted magnetic moment, the bandwidth used, the conductivity of the subsurface and the signal/noise ratio (Spies 1989). AEM data were processed by following the procedure described in Reninger et al. (2020), which is based on the use of the singular value decomposition (Reninger et al. 2011). The aim of the applied processing was to keep as much resolution as possible (Reninger et al. 2020).

Finally, a manual editing procedure was performed, mainly to remove remaining inductive/galvanic coupling noises. In order to improve the coverage of the dataset, good quality portions of ferry lines (helicopter routes between each flight line departure and between the airport and each day first flight line departure) were also considered during the processing (Reninger et al. 2020). Data were then inverted in "smoothed" one-dimensional (1D) models using a quasi-3D spatially constrained inversion (SCI) algorithm (Viezzoli et al. 2008). Each 1D model displays the resistivity variations with depth. More 2D information can be obtained, interpolating the resistivity layers falling into a depth or elevation range. This step is generally repeated over the entire range of investigation. The obtained slices can then be merged to build a 3D resistivity model allowing drawn sections in any direction and extraction of interfaces and/or volumes.

Water budget calculation

A hydrological water budget model of Martinique has been implemented (Vittecoq et al. 2007; Arnaud and Lanini 2014; last update: Taïlamé and Lanini 2020) for water stakeholders in order to assess water resources and water withdrawals. This model allows daily to inter-annual water budget calculations at the watershed or subwatershed scale. This lumped type hydrologic model requires meteorological data series: rainfall rate and potential evapotranspiration, spatialized at

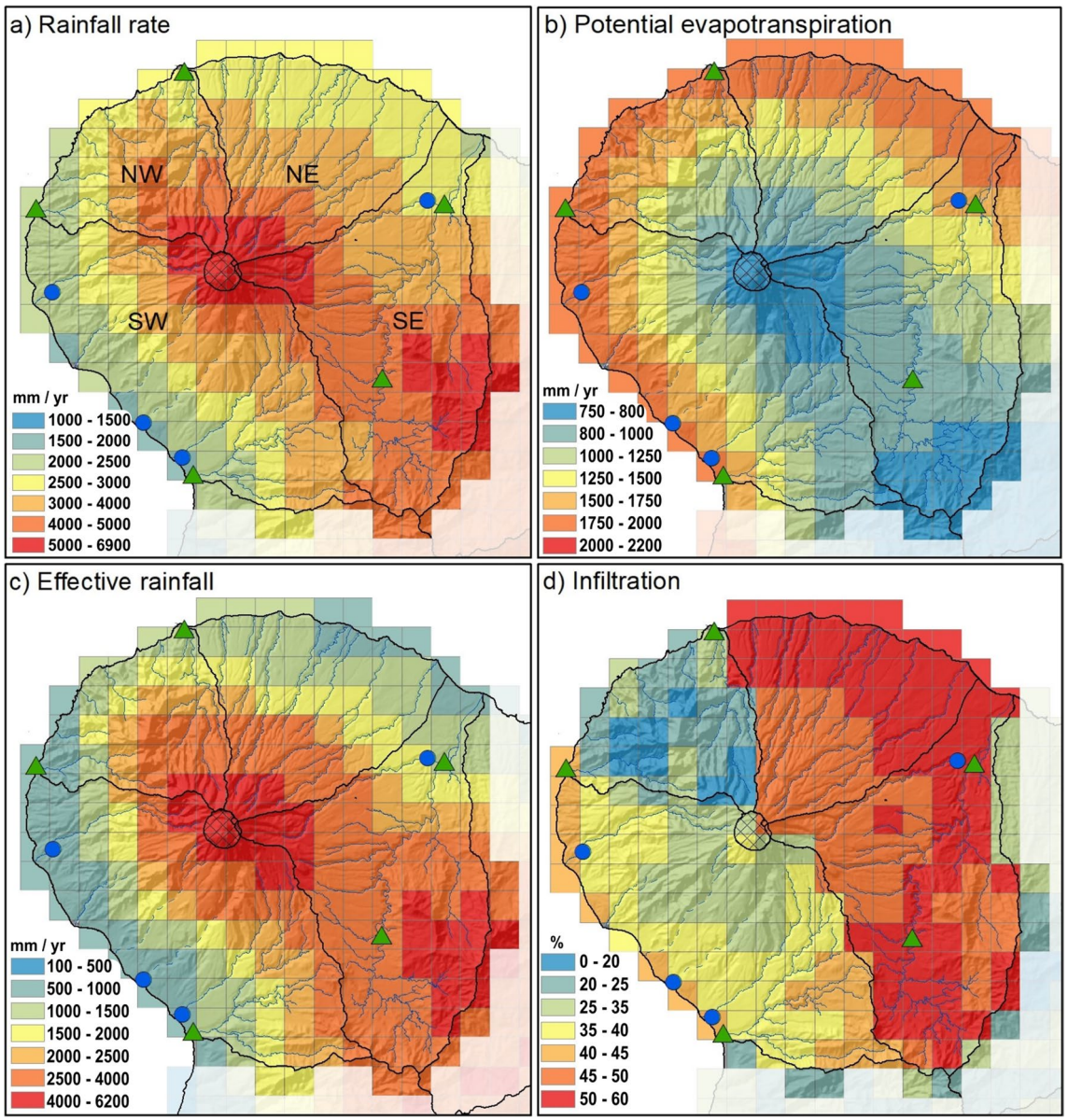

Fig. 4 Water budget calculation results at the square kilometer scale: **a** Rainfall rate, **b** Potential evapotranspiration, **c** Effective rainfall, and **d** Infiltration ratio. Blue dots correspond to groundwater level monitoring points and green triangles to river flowrate monitoring stations, whose data have been used for model calibration (Taïlamé and Lanini, 2020). NW, NE, SE, SW and the gridded summit zone correspond to the areas reported in section "Water budget"

a 1–km^2 grid, as well as time series related to water surface and groundwater withdrawals. A cultural map, soil-water-capacity map and runoff coefficient map at the kilometer scale are also needed as input data to calculate the effective rainfall, real evapotranspiration, infiltration/runoff ratio, flow rate at the outlet of rivers and the groundwater level in the underlying aquifers. In this model, Martinique Island has been divided into 1,206 cells, of which 227 concern Montagne Pelée and connected catchments. In each square kilometer cell, the exponential drainage of the soil reservoir is divided between runoff (fast surface and subsurface flow) and infiltration (slower flow to the underlying first aquifer) considering two parameters—the runoff coefficient and the transit time. Runoff and infiltration flow from each square kilometer cell should then be aggregated at the catchment or subcatchment scale. The last model calibration was carried out (Taïlamé and Lanini 2020) by comparing the results of the model (flowrate at the outlet of rivers and groundwater level) with data from the river flowrate monitoring network and piezometric level monitoring network over the period 1991–2017. The calibration parameters at the square-kilometer-cell scale (soil reservoir drainage time and runoff

coefficient) and at the catchment scale (underground reservoir drainage time and porosity) are adjusted to optimize the model results.

In this research, Montagne Pelée has been divided into five areas: (1) a north-western zone corresponding to watersheds located on the first-stage geological unit, (2) a northeastern zone and, (3) a southwestern zone, both corresponding to the opposite volcano flanks dominated by the 2nd and the 3rd stage geological units, (4) a southeastern zone corresponding to the Capot River watershed whose particularity is to be half on Montagne Pelée deposits and half on the Morne Jacob andesitic rocks (2.2–5.5 Ma) and, (5) a small zone corresponding to the summit zone (Fig. 4). Rainfall, real evapotranspiration, effective rainfall and infiltration have then been extracted for each area. A schematic view of the model is shown in Fig. SI_4 in the ESM.

Results

Resistivity ranges of pyroclastic aquifers and the main geological units

AEM results correlated with boreholes and springs data allow one to identify unsaturated zones, aquifers, and seawater intrusions as well as the main geological units. Eight characteristic cross-sections are presented in Figs. 5 and 6 and their locations are shown in Fig. 2 (and Figure SI 3 in the ESM). The main units highlighted are the following:

- Ranging between 50 and 1000 ohm.m, pyroclastic deposits are particularly well imaged. Within this resistivity range, three subsets can be distinguished:
  - The higher resistivity values (>300 ohm.m) correspond to unsaturated and unweathered to slightly weathered pyroclastic deposits and are highlighted by "1" on Figs. 5 and 6.
  - Resistivities between 70 and 300 ohm.m correspond to aquifers, confirmed by water level data in boreholes or the position of springs and are highlighted by "2" on Figs. 5 and 6. The higher aquifers values, ranging between 200–300 ohm.m, are observed for the "Pecoul" area and are highlighted by "3" on the C2 cross-sections (Fig. 5) and C6 (Fig. 6). Surficial aquifers of limited extent within 3rd stage pyroclastic deposits, with low flowrate springs, are highlighted by "4" in Figs. 5 and 6.
  - Lower values, ranging between 50 and 70 ohm.m, are observed on the southwestern volcano flank between the Claire River and the Sèche River (highlighted by "5" on the C1 cross section on Fig. 5). This 50–100-m-thick layer is interpreted as mineralized (1,100–1,400 µS/cm) and warm (30–32 °C) groundwater.
- Below 50 ohm.m, two geological units, located below the pyroclastic deposits, are imaged:
  - On the northwestern side of the volcano, with resistivity around 50 ohm.m, andesitic formations from the first stage (highlighted by "6" on Figs. 5 and 6),
  - On the southeastern side, with resistivity below 30 ohm.m, andesitic formations from the Morne Jacob volcano (highlighted by "7" on Figs. 5 and6).
- Resistivities lower than 15 ohm.m are observed around the coastal boundary of the volcano and correspond to seawater intrusions (highlighted by "8" on C1, C3 and C7 cross-sections on Figs. 5 and 6).

Hydrogeological characteristics

Transmissivity values, calculated thanks to pumping tests conducted in 21 boreholes, varies between 9 10^{-5} and 8 10^{-2} m^2/s, with 1 10^{-3} and 6 10^{-3} m^2/s as the 1st and 3rd quartiles and with 2 10^{-3} m^2/s as the mean value. Hydraulic conductivity values, calculated by dividing transmissivity by the thickness of aquifer crossed by each borehole (Fig. 7), varies between 2 10^{-6} and 3 10^{-3} m/s, with 6 10^{-5} and 3 10^{-4} m/s as the 1st and 3rd quartiles and 2 10^{-4} m/s as the mean value. The harmonization of geological descriptions and ages of aquifers crossed by each borehole, thanks to the new geological history classification (Boudon and Balcone–Boissard 2021), allows a clear correlation between hydraulic conductivities and ages (Fig. 7): the older the unconsolidated pyroclastic deposits are, the lower their hydraulic conductivity.

Only three storage coefficients have been reported. The higher value is 4 10^{-1} in the younger pyroclastic aquifer on the southwestern flank (1,902 PDC deposits, 3rd stage, 2nd part). The lower is 3 10^{-4} in clayey PDC, 4,400 years before on the northeastern flank (3rd stage, 2nd part) and should be the result of the rapid weathering of pyroclastic deposits due to the higher rainfall exposition of this flank. A middle value of 2 10^{-3} in low silica subplinian–plinian deposits is also reported on the northeastern flank (3rd stage, 1st part).

Piezometric levels, measured in the boreholes intersecting water inflows, show two groups. The first one is composed of 16 boreholes located on the southwestern volcano flank (Fig. 8), between 8 and 80 m amsl, close to the sea with a maximum distance of 1,200 m from the coast and a hydraulic gradient of 2.2%. Water levels measured in these boreholes, generally below the level of the rivers, suggest that the rivers are infiltrating towards the aquifer. The second set is composed of 18 boreholes located on the northeastern volcano flank (Fig. 9), between 16 m and 614 m amsl, with water

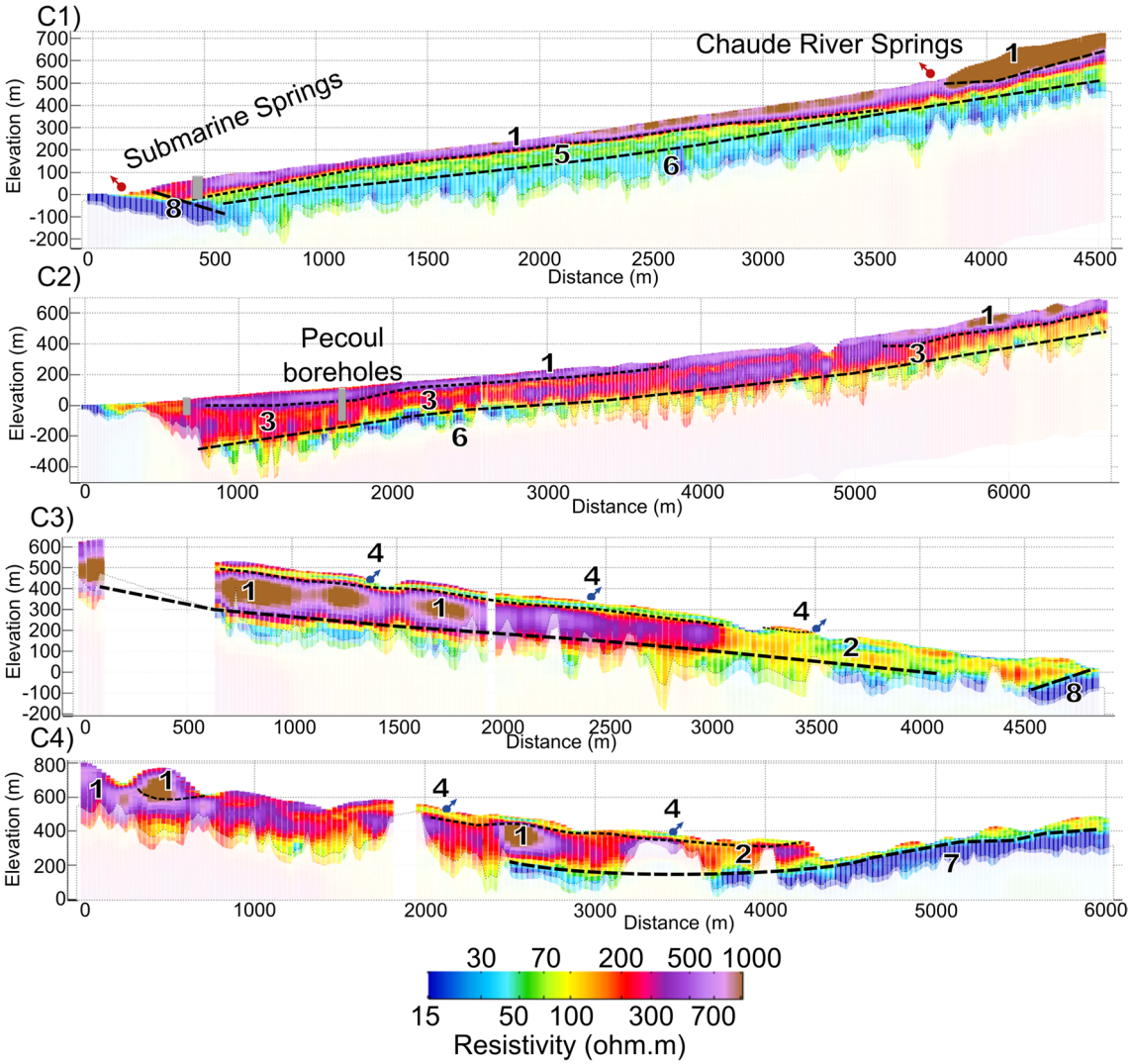

Fig. 5 Internal resistivity and hydrogeological structures along cross sections C1, C2, C3 and C4. The locations of the cross sections are shown on Fig. 2. Legend: (1) unsaturated and unweathered to slightly weathered pyroclastic deposits (>300 ohm.m), (2) aquifers (70–300 ohm.m), (3) 'Pecoul' aquifer (200–300 ohm.m), (4) limited extension superficial aquifers within 3rd stage pyroclastic deposits, (5) mineralized (1,100–1,400 µS/cm) and warm (30–32 °C) aquifer (50–70 ohm.m), (6) andesitic formations from the first stage (<50 ohm.m), (7) andesitic formations from Morne Jacob Volcano (<30 ohm.m), (8) seawater intrusions (<15 ohm.m)

level depth a few tens meters below ground level (mean: 41 m, min: 3 m, max: 97 m,) and a mean hydraulic gradient of 5.7%. Half of the boreholes have water level above the river level and the other half below, allowing distinguishing sectors with perched aquifers, sectors where groundwater flows towards rivers and sectors where rivers flow to the aquifer.

Freshwater springs are mainly located between 110 and 440 m (1st and 3rd quartile) with 280 m as the mean elevation. The two higher springs are at 900 and 950 m amsl. Most springs have low flowrates (1–10 m^3/h) except one with higher flowrate (Morestin spring ≈ 200 m^3/h). Almost all springs (90%) are on the northeastern volcano flank (Fig. 9). On this northeastern flank they can be classified into three equivalent distribution groups (Fig. 9b). The first group corresponds to springs situated in the river's bed, intersecting the basal aquifer water table (depression spring type 1, Fig. 9). The second group corresponds to springs located in the middle part of the steep slopes of the river incisions, corresponding also to perched aquifers of limited extent, emerging thanks to paleosols or geological discontinuities (contact spring type 2, Fig. 9). The third group corresponds to springs located on the gentle slopes of the volcano flanks, corresponding to small-extension perched aquifers with subsurface flows and superficial water tables (depression spring type 3, Fig. 9). On the southwestern flank of the volcano (Fig. 8), the dozen springs are located in the upper part of watersheds (>4,000 m from the sea) and emerge from

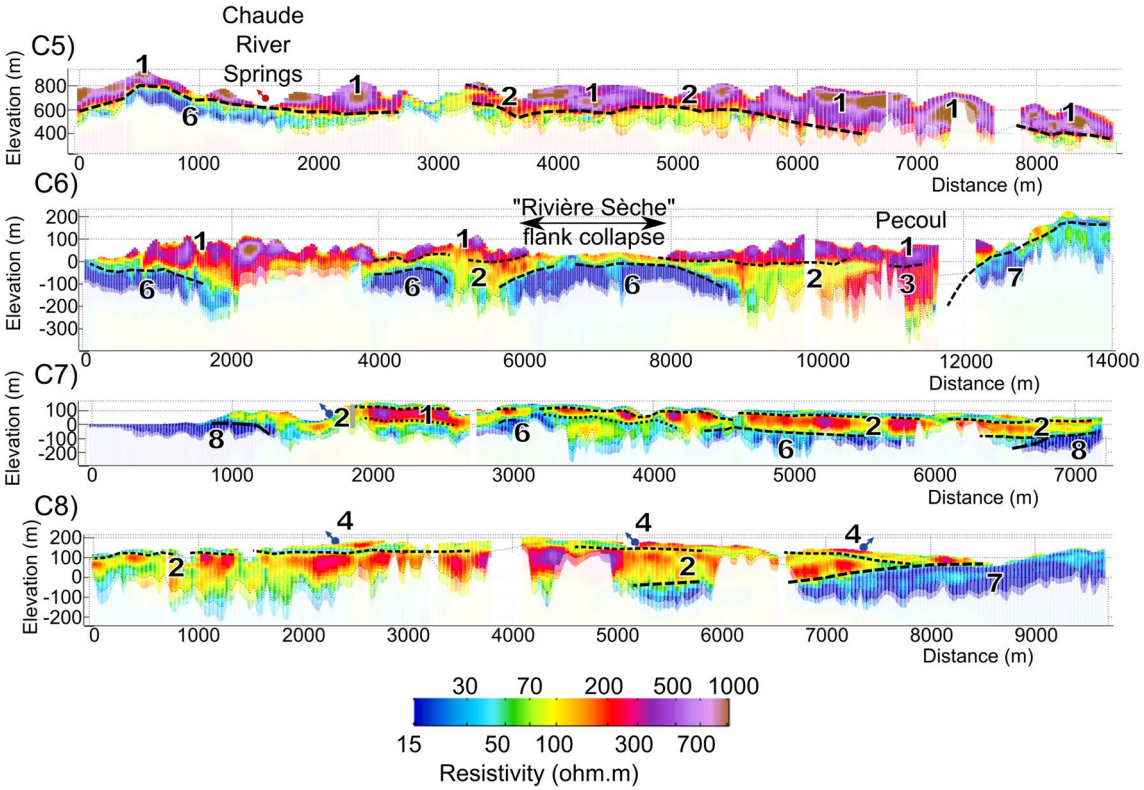

Fig. 6 Internal resistivity and hydrogeological structures along cross sections C5, C6, C7 and C8. The locations of the cross sections are shown on Fig. 2. Legend: (1) unsaturated and unweathered to slightly weathered pyroclastic deposits (>300 ohm.m), (2) aquifers (70–300 ohm.m), (3) 'Pecoul' aquifer (200–300 ohm.m), (4) limited extension superficial aquifers within 3rd stage pyroclastic deposits, (5) mineralized (1,100–1,400 µS/cm) and warm (30–32 °C) aquifer (50–70 ohm.m), (6) andesitic formations from the first stage (<50 ohm.m), (7) andesitic formations from Morne Jacob Volcano (<30 ohm.m), (8) seawater intrusions (<15 ohm.m)

perched aquifers. Three of these springs are located near the summit, the Samperre spring is located at the bottom of a large landslide (Peruzzetto et al. 2022), and the eight other springs are located east from the Roxelane River, outside of the flank collapses structures. Lastly, all (except one) of the thermal springs of the Montagne Pelée are also located on this southwestern flank.

Water budget

Results of the water budget calculation (rainfall, evapotranspiration, effective rainfall, runoff and infiltration) for the five zones and the Montagne Pelée Volcano (Fig. 4) are given in Table 1. Water balance calculations show that, at the volcano scale, mean annual rainfall is 3,639 mm, mean annual potential evapotranspiration is 1,282 mm, mean annual effective rainfall is 2,456 mm and mean annual infiltration is 1,099 mm, corresponding to an annual groundwater recharge volume of 209 Mm^3 (almost five times the annual drinking-water need for the island). Depending on the intensity of the rainy season, the interannual variability can be high with a maximum annual value reaching 6,861 mm for rainfall and 6,103 mm for effective rainfall. At the volcano scale, mean infiltration is 45% of effective rainfall and mean runoff is 55%. Depending on the watershed location, mean infiltration varies between 35 and 52% of the effective rainfall (and runoff between 48 and 65%).

Water budget results calculated on the northeastern flank with a repartition between 51% of infiltration and 49% of runoff are in agreement with Barat (1986) who calculated an infiltration rate of 50% (varying between 40 and 60% depending on the watershed). On the southwestern flank, with a repartition between 35% of infiltration and 65% of runoff, the results here are also in agreement with Barat (1986) who calculated an infiltration rate of 38 and 62% of runoff for the Roxelane River. The annual groundwater recharge volume is then greater on the southwestern flank (49 Mm^3) than on the northeastern flank (42 Mm^3).

Seawater intrusions

The coastal fringe of the aquifers of this volcanic edifice is hardly affected by seawater intrusions. C1 and C3 cross-sections (Fig. 5) show very low resistivity values (<3 ohm.m)

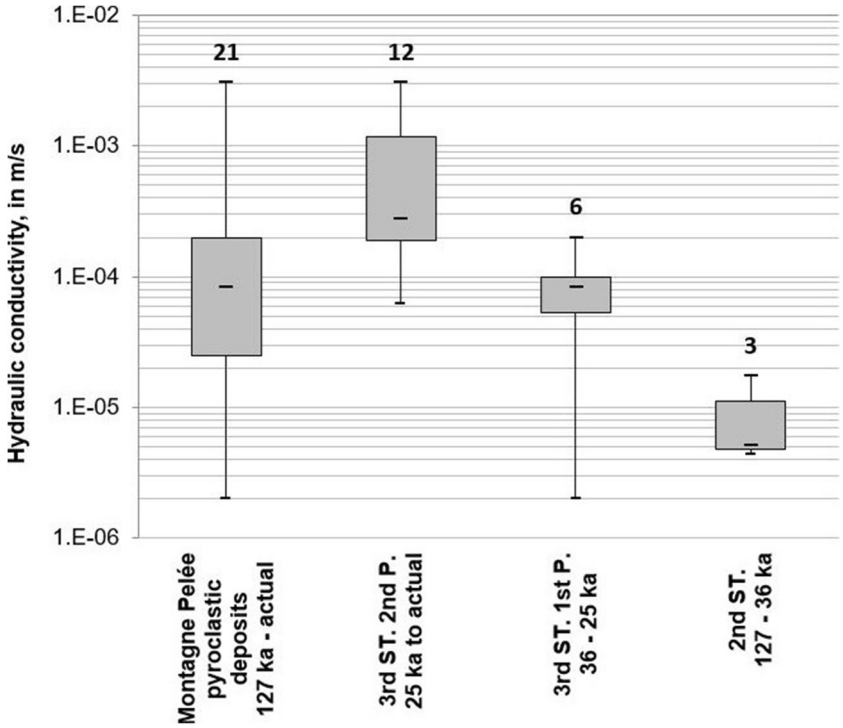

Fig. 7 Comparison between hydraulic conductivity and pyroclastic deposit ages for 21 boreholes in which pumping tests have been conducted. The older the pyroclastic deposits, the lower their hydraulic conductivity

in the sea, corresponding to marine saline water and resistivity values <10–15 ohm.m in the continuity inland. These cross-sections are representative of the slope of the seawater intrusions (SWI) on most of the others around the volcanic edifice. With a slope of about –40%, SWI rapidly reaches depths of up to 100 m within a few hundred meters from the coast, which is deeper then the DOI via the SkyTEM 304 system. This strong SWI slope is consistent, considering the strong groundwater recharge rate and the aquifer's water-table slopes higher than 2%. Electrical conductivity

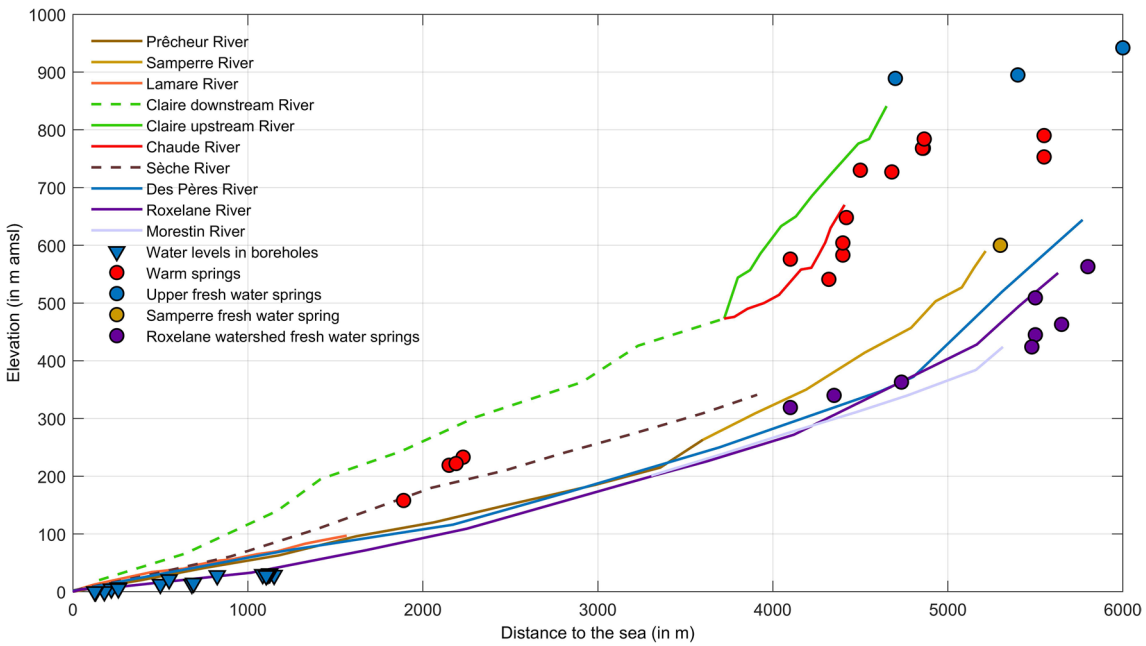

Fig. 8 Topographic profiles of the Montagne Pelée southwestern flank rivers with piezometric levels in the boreholes and elevations of the freshwater springs and thermal springs

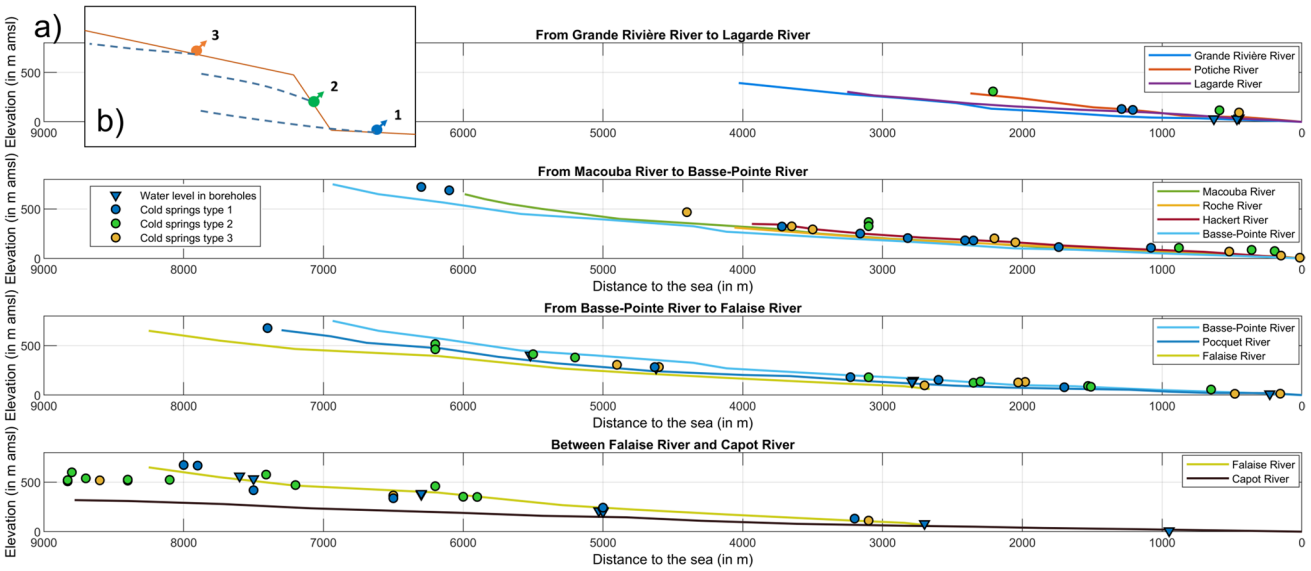

Fig. 9 **a** Topographic profiles of the Montagne Pelée northeastern flank rivers, with piezometric levels in the boreholes and elevations of the freshwater springs. Inset **b** shows the vertical arrangement of spring outflows

measurements in the three closest boreholes to the coast are also in agreement (153, 280 and 418 µS/cm for distances between 150 and 300 m from the coast).

Montagne Pelée hydrogeological conceptual model

Correlation between the 3D resistivity model and hydrogeological data from boreholes and springs allows for a description of the hydrogeological conceptual model of the Montagne Pelée volcano. Figure 10 presents a schematic view of the hydrogeological conceptual model, along a theoretical southwest–northeast axis. In addition to the hydrogeological structure of the first hundred meters, this model also shows, thanks to magneto telluric data (Gadalia et al. 2014), the cap rock, the supposed hydrothermal system and the upper crust.

The upper perched aquifer

The upper aquifer is a perched aquifer (Fig. 10 and the zoom labelled A) located within the recent lava domes (3rd stage, 2nd part). These andesitic domes are deeply fissured and fractured, and the upper part of the volcano between the domes is a chaos of blocs allowing fast infiltration of the huge amount of effective rainfall on the top of the volcano (mean annual amount: 5,813 mm, corresponding to about 7.5–12 Mm^3, depending on the surface area considered). Furthermore, an endorheic topography is observed between the bottom of the domes and the crater rim (elevation 1,200 m), also allowing a fast infiltration of rainfall. The area of this aquifer is difficult to determine precisely but is about 1–2 km^2. The thickness of the saturated zone is unknown, but it is supposed that the thickness is small, as spring flowrates are low and water is expected to infiltrate at depth toward the deep hydrothermal system.

Table 1 Water budget calculation results for rainfall, evapotranspiration, effective rainfall, runoff and infiltration for all five zones and the Montagne Pelée Volcano

	Area (km^2)	Rainfall (mm)	PET (mm)	Effective rainfall (mm)	Infiltration (mm)	Runoff (mm)	% Infiltration	Infiltration (Mm^3)
NW	26.2	3,586	1,478	2,246	820	1,420	37%	22
NE	39.8	3,417	1,470	2,050	1,052	994	51%	42
SW	65.9	3,227	1,271	2,109	745	1,358	35%	49
SE	58.7	4,275	1,079	3,216	1,652	1,556	52%	97
Summit	1.3	6,571	754	5,813	-	-	-	-
Volcano scale	190.6	3,639	1,282	2,456	1,099	1,351	45%	209

The other aquifers can be categorized into three groups—the northeastern flank aquifers, the southwestern flank aquifer and the southeastern flank aquifers. The northwestern quarter of the volcano, characterized by first-stage primitive Montagne Pelée lavas flows, remains little known, as only one hiking trail exists near the coast, across the tropical forest, and wind conditions and rough topography did not allow the helicopter-borne survey.

The northeastern flank aquifers

The northeastern flank is characterized by two types of aquifers (Fig. 10 and the zoom labelled B). In the first 10 m below ground level, small perched aquifers, within pyroclastic deposits of the third stage, give rise to low flowrate springs at various elevations (mainly between 100 and 400 m amsl). Beneath is a second aquifer (second-stage pyroclastic deposits and third stage, with the first part being pyroclastic deposits), corresponding to the basal aquifer flowing to the sea. This basal aquifer is also found at greater elevations (200–400 m amsl) at greater depths (200 m) depending on the morphology and the elevation of the first part lava and breccia located below.

The southeastern flank aquifer

The geomorphology of the southeastern flank differs from the northeastern flank. At similar elevations to the northeastern flank, pyroclastic deposits, mainly from the third stage, only have a maximum of 200 m thicknesses. These deposits lie on the first stage and the Morne Jacob andesitic lavas which outcrop in some river beds. In the first 10 m, small perched aquifers give rise to low flowrate springs. Under these small aquifers is found the main aquifer of the flank, in which groundwater flows are controlled by (1) the topography of the first stage and Morne Jacob andesitic rocks, and (2) the incision of the Capot River and its tributaries within the pyroclastic deposits (C4 cross-section on Fig. 5). Due to this geomorphology, important groundwater drainage by the river gives the latter the higher flowrate of the island.

The southwestern flank aquifers

The southwestern flank has several distinctive characteristics. The first particularity is its geomorphology, marked by horseshoe shape relief resulting from two flank collapses (127 ka and 36 ka), as exposed by Le Friant et al. (2003) and Boudon and Balcone-Boissard (2021). The 36-ka Rivière Sèche event is then particularly visible on the C6 cross-section (Fig. 6): several tens of meters of pyroclastics deposits are missing and the basis of the collapse should have been controlled by the lava from the first stage. The basis of the 127-ka event is less obvious, but well visible on its southern rim (C6 cross-section, Fig. 6). It is reasonable to think that this event may not have happened all at once, but may be the result of successive collapses. Around 20 boreholes have been drilled inside these two structures and crossed mainly the third-stage deposits, enabling identification of a continuous basal aquifer. A deepening of the andesitic lavas (below 50 ohm.m) and consequently an increasing thickness of 200 m of saturated pyroclastic deposits is visible in the axis of the Pecoul sugarcane field (C2 and C6 cross-sections). The extension of this deepening does not correspond to the actual identified flank collapse horseshoe shape's structure and could then correspond to (1) an unknown masked structure or (2) the result of river erosion over thousands of years before being filled by pyroclastic deposits.

The second hydrogeological particularity of the southwestern flank is the quasi absence of small-perched aquifers at various elevation, as observed on the eastern flank, that can be linked to the effect of the successive flank collapses which have not preserved the structures that allow the existence of these small aquifers. The Morestin spring, the higher flowrate spring of the volcano and seven other springs (Fig. 8), located between 4,000 and 6,000 m from the sea and at an elevation between 300 and 600 m, are outside the flank collapse structures and should be associated with a perched aquifer. The third hydrogeological particularity of the southwestern flank is the presence of warm springs, testifying to the existence of a hydrothermal system at depth.

The fourth hydrogeological particularity is the complete infiltration of warm water from the Claire River around 500 m elevation and between 400 and 500 m elevation for the Chaude River, and the existence of mineralized groundwater downward flows particularly visible on the geophysical data (cf. C1 cross-section, Fig. 5). The hydrogeological functioning of this area is synthetized in Fig. 11, with the representation of the lateral extension of the 50 ohm.m layer and color scale according to the elevation of the top of the geophysical layer. Thermal water from the Claire and Chaude rivers infiltrates in highly permeable pyroclastic deposits (3rd part, 2nd stage: 1902–1905 and 1929–1932 PDCs deposits, also known as the "Coulee Rivière Blanche") and flows toward the sea following the morphology of the flank before the 1902 eruptions. Thermal springs at shallow depth near the shore and the thermal well near the coast confirm this hypothesis.

The aquitard bedrock

Finally, the hydrogeological aquitard bedrocks of the basal aquifers are the first-stage primitive Montagne Pelée (Mont Conil) lava flows of approximately two thirds in

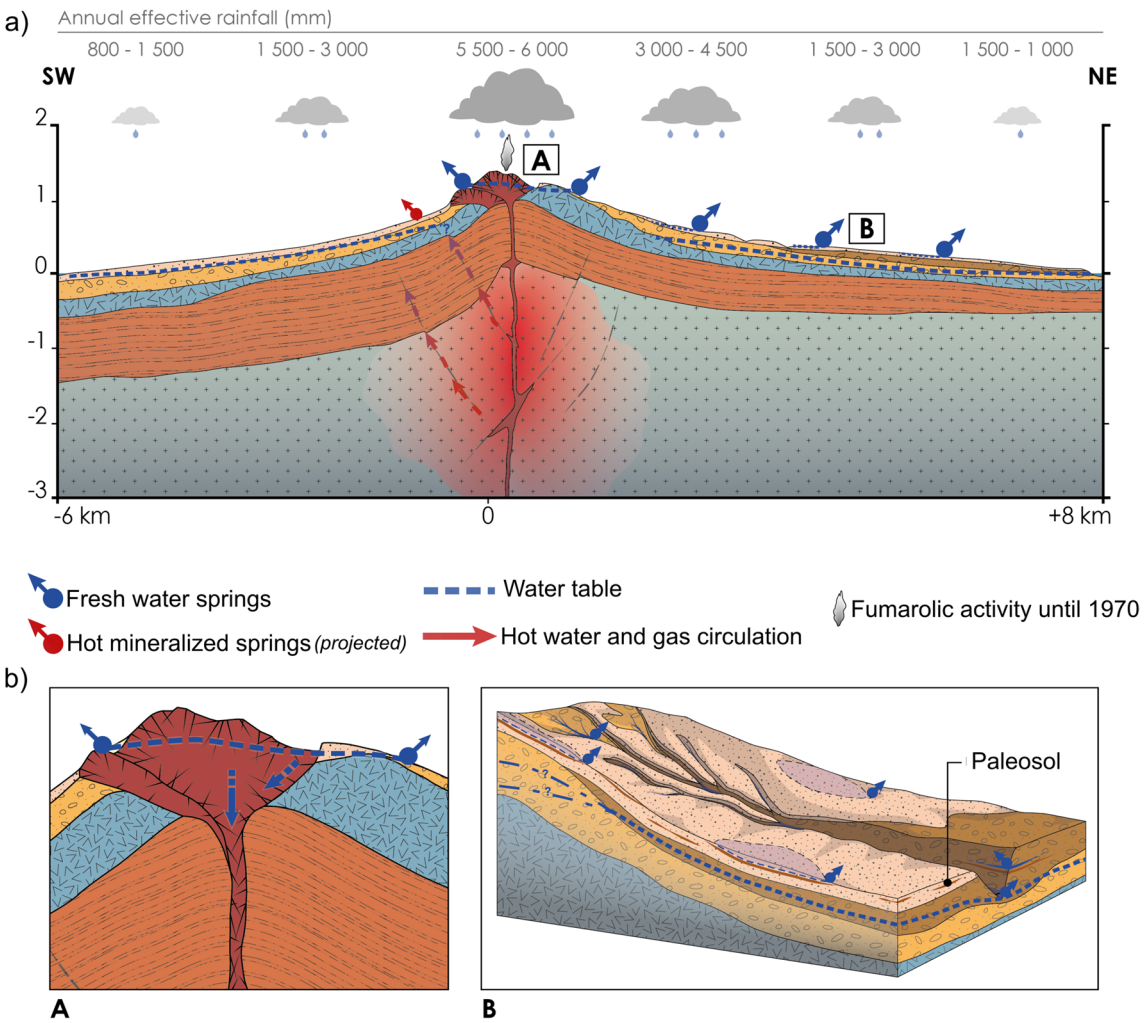

Fig. 10 **a** Hydrogeological conceptual model of the Montagne Pelée volcano as a SW–NE cross section, **b** enlargements for A (summit) and B (NE slope) and **c** hydrogeological log with geological units and associated stage of building, hydraulic conductivity and resistivity

the northwest direction and the Morne Jacob andesitic lavas of the remaining third in the southeastern direction. Even if the hydraulic conductivity of these lavas is unknown, one can consider that the hydraulic conductivity contrast between the highly permeable pyroclastic deposits and the weathered lavas flows (considering their low electromagnetic resistivity) is enough to play the role of an aquitard bedrock.

Discussion

The hydrogeological conceptual model of the Montagne Pelée volcano has been defined thanks to the correlation of rarely available datasets on the same edifice—helicopter-borne electromagnetic data with a high resolution, a relatively high borehole density database, with water level and hydraulic conductivity data, and a spring database. The results, highlighting thick permeable pyroclastic deposits along the volcano flanks, should help researchers to better understand the hydrogeological functioning on the proximal (2–10 km) part of an andesitic stratovolcano, following the description of Vessell and Davies (1981), Bogie and Mackenzie (1998) and Selles et al. (2015). This model, nevertheless, could not be extrapolated to the rest of Martinique Island, as pyroclastic deposits only concern the Montagne Pelée. In the central part of Martinique Island, two other conceptual models have been developed at a watershed scale (Vittecoq et al. 2019) and an aquifer scale (Vittecoq et al. 2015). At the Lesser Antilles scale, the classification of high-rise volcanic islands into three categories by Robins et al. (1990) should be updated with the detailed description given here.

The southwestern flank collapses have affected the geological evolution of the Montagne Pelée and have induced a structural difference between the northeastern and the southwestern flanks (Vincent et al. 1989; Le Friant et al. 2003; Boudon and Balcone-Boissard, 2021). These flank collapses are due to an eastern-western topographic asymmetry of the volcano with steeper on-land and underwater slopes in the western flank. This structural asymmetry is reflected in its hydrogeological functioning with perched aquifers and springs on one side and none on the other. Similar observations are expected on other volcanos as flank collapses due to the asymmetry of the volcano have been noticed on some others, whether in the West Indies (Soufriere of Saint Lucia and Soufriere of Saint Vincent (Boudon et al. 2007) or at the smaller-scale Soufriere of Guadeloupe (Rosas Barbajal et al. 2016) in USA (Mount Saint Helen, Lipman and Mullineaux 1981) or in Indonesia (Mount Merapi, Selles 2014). The Merapi volcano is for instance marked by a stable east flank with springs and perched aquifers, whereas the western flank is destabilized by recent eruptions and without springs (Selles 2014). These flank collapses induced a rejuvenation of the geomorphology by thick pyroclastic deposits and a weaker incision. Thus, associated aquifers remain hidden and do not allow springs outflow. As demonstrated

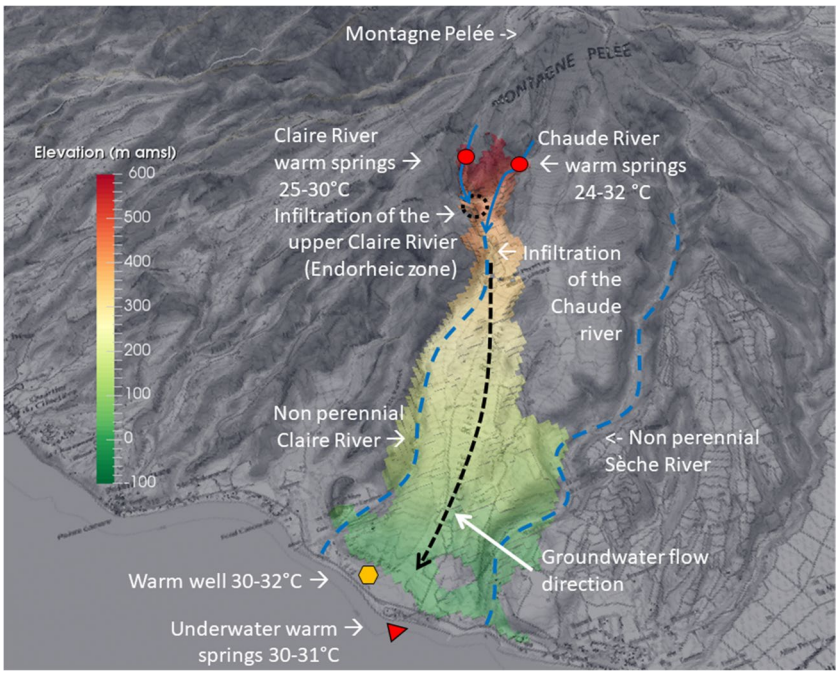

Fig. 11 Interpreted pseudo-3D view of the mineralized (1,100–1,400 µS/cm) and warm (30–32 °C) aquifer (50–70 ohm.m), with representation of the lateral extension of the 50–70 ohm.m layer, with color scale according to the elevation of the top of the geophysical layer

with the hydraulic conductivity dataset for Montagne Pelée, the younger the pyroclastic deposits are, the higher their hydraulic conductivity. The decrease of hydraulic conductivity as a function of time should be the result of weathering processes. If there is enough rainfall, significant aquifers are expected within flank collapses, as supported by self-potential measurements (Zlotnicki et al. 1998) showing the floor of the horseshoe-shaped structure. Conversely, the opposite flank should present a superposition of increasingly old deposits with decreasing hydraulic conductivity and lower storage coefficient. Paleo-soil, erosion and weathering processes (Rad et al. 2013) between each eruptive sequence also lead to horizontal discontinuities with lower permeability, allowing perched aquifers and associated springs. Lastly, helicopter-borne electromagnetic data probably show another horseshoe structure below the Pecoul sugarcane field masked by pyroclastic deposits filling.

Hydraulic conductivity values of the Montagne Pelée pyroclastic deposits, with 2 10^{-4} m/s as mean value, are on the same order of magnitude as Mount Mazama in the Oregon Cascade Range, USA (Aldous and Gurrieri 2011), with measured average hydraulic conductivity of plinian pumice layers at 1.4 10^{-4} m/s. These values also match with fine sand or gravel hydraulic conductivity, according to Domenico and Schwartz (1990), facilitating the similarities in order to better explain groundwater flows to the public and stakeholders.

Groundwater also plays a key role in phreatic eruptions. The previous eruption cycles at Montagne Pelée (1902–1905 and 1929–1932) started with phreatic eruptions. In 1792 and 1851, phreatic eruptions were also reported, without having been followed by magmatic eruptions. Each time, fumaroles activity is noticed before phreatic eruptions with a rapid decrease after each eruption cycle (Barat 1986). This fumaroles activity should be evidence that the upper-perched aquifer is alternatively heated by conduction from deeper magma and by magmatic gas when the magma rises (going until boiling then vaporized when phreatic eruption occurred) and acting as a buffer against rising gas when the eruption stops. The rapid decrease of fumaroles activity is also evidence that the aquifer rapidly "refills" thanks to the high quantity of effective rainfall thus cooling and diluting the effect of the magmatic gas.

It is assumed that the recharge of the hydrothermal system, located between 1.5 and 3 km depth, is via deep vertical groundwater flow restricted to the central crater system (Traineau et al. 1989; Zlotnicky 1998; Gadalia et al. 2014). The results here show that the upper perched aquifer gathers rainfall from the endorheic system within the crater. The low real evapotranspiration rate, together with a weak runoff, favours a high infiltration rate. The springs' low flowrates from this upper aquifer and the interpreted structure of the first stage of edification confirmed this hypothesis, but the "connection" with the hydrothermal system remains unclear as the upper magma pathway is supposed to be a maximum of a few tens of meters (corresponding to the diameter of the lava spine) and sealed. Furthermore, the cap rock identified by magneto telluric data (Gadalia et al. 2014) pressurized the hydrothermal system, with few leaks (along potential fractures) leading to the existing thermal springs and past fumaroles. Deep infiltrated water should then refill the hydrothermal system only if the pressure of the water height in the upper aquifer and the supposed fractures near the plumbing system is higher than the pressure of the hydrothermal system. Better knowledge of the hydrothermal system extension and pressure is needed to more deeply characterize the relationship with the shallow aquifer.

Conclusion

The hydrogeological conceptual model of the Montagne Pelée Volcano has been defined thanks to the correlation of rare data on the same volcanic massif—helicopter-borne electromagnetic data with a high resolution, a relatively high density of boreholes with water level and hydraulic conductivity data, and a spring database. The study has also demonstrated that the older the pyroclastic deposits, the lower their hydraulic conductivity. The on-land and underwater asymmetric topography of the volcano has induced flank collapses leading to a structural difference between the northeastern and southwestern flanks, as reflected in its hydrogeological functioning. Finally, this paper discusses relationships between past phreatic eruptions and the hydrothermal system.

The way forward now is to describe the geochemical characteristics of these multiple aquifers, to more deeply characterize the structure of the volcano below the DOI of the geophysical survey (≈200 m), in order to build a 3D geological and hydrogeological model at the volcano scale and to improve understanding of groundwater flows at the scale of each flank.

Appendix 1

Table 2 Borehole database (WGS84 coordinate system)

National number	City	Boreholes name or locality	X (m)	Y (m)	Borehole elevation (m)	Borehole depth (m)	Water level elevation (in m amsl)	T (m^2/s)	K (m/s)	Aquifer geology
1165ZZ0001	Grand Rivière	F1	696,316	1,644,519	30	36	26	1.0E-03	5E-05	3rd ST. 1st P.
1165ZZ0012	Grand Rivière	F4	696,276	1,644,549	30	15	26	1.0E-03	1E-04	3rd ST. 1st P.
1165ZZ0013	Grand Rivière	F5	696,285	1,644,546	30	15	26	2.0E-03	2E-04	3rd ST. 1st P.
1165ZZ0014	Macouba	Beauséjour BR1	696,717	1,644,902	136	160	39	-	-	-
1166ZZ0004	Basse Pointe	Vivé P3	705,586	1,642,059	16.5	30	14.5	-	-	-
1166ZZ0026	Basse Pointe	Chalvet	705,086	1,643,059	30	29	12	-	-	-
1166ZZ0027	Grand Rivière	F2	696,272	1,644,570	30	40	26	2.0E-03	1E-04	3rd ST. 1st P.
1166ZZ0028	Grand Rivière	F3	696,265	1,644,576	30	15	26	7.0E-04	7E-05	3rd ST. 1st P.
1166ZZ0055	Basse Pointe	Leyritz	702,503	1,642,166	165	28	149	-	-	-
1166ZZ0056	Basse Pointe	Leyritz	702,652	1,641,980	163	41	134	-	-	-
1166ZZ0057	Basse Pointe	Leyritz	701,871	1,641,560	230	50	-	-	-	-
1166ZZ0059	Macouba	Loucou CHE1	698,380	1,643,494	259	160	147	2.4E-04	5E-06	2nd ST.
1166ZZ0060	Macouba	Perpigna PE2	698,450	1,644,928	125	150	31	1.2E-03	2E-05	2nd ST.
1166ZZ0061	Macouba	Potiche PR1	697,705	1,645,101	120	145	30	1.9E-04	4E-06	2nd ST.
1167ZZ0008	Saint Pierre	Fond Canonville	693,856	1,635,229	63	50	28	6.0E-03	3E-04	3rd ST. 2nd P.
1167ZZ0021	Saint Pierre	Fond Corre 1	695,536	1,632,379	29	50	5	3.1E-02	1E-03	3rd ST. 2nd P.
1167ZZ0022	Saint Pierre	Fond Corre 2	695,726	1,632,589	55	60	13	1.1E-02	6E-04	3rd ST. 2nd P.
1167ZZ0023	Saint Pierre	Coulée Rivière Blanche	694,666	1,633,319	24.23	60	0.23	4.4E-02	1E-03	3rd ST. 2nd P.
BSS003QEGW	Saint Pierre	Coulée Rivière Blanche CB1	694,574	1,633,484	57.7	82	-	-	-	-
1167ZZ0024	Precheur	Piézomètre BRGM	691,446	1,637,549	49	50	13	3.0E-03	2E-04	3rd ST. 2nd P.
1167ZZ0027	Saint Pierre	Fond Canonville	693,436	1,634,839	22	20	7	-	-	-
1167ZZ0028	Saint Pierre	Fond Canonville	693,636	1,635,049	48	40	21	-	-	-
1167ZZ0029	Saint Pierre	Amont CDST	696,266	1,632,119	57	63	15	1.5E-03	7E-05	3rd ST. 2nd P.
1167ZZ0031	Saint Pierre	Pecoul	696,881	1,631,966	73	73	30	3.0E-02	1E-03	3rd ST. 2nd P.
1167ZZ0035	Saint Pierre	Tombeau des Caraïbes SC4	694,196	1,634,499	55	20	-	-	-	-
1167ZZ0036	Saint Pierre	Tombeau des Caraïbes SC5	693,926	1,634,279	100	20	-	-	-	-
1167ZZ0037	Saint Pierre	CET Fond Canonville	693,133	1,634,897	8.03	20.5	0.03	-	-	-
1167ZZ0038	Saint Pierre	CET Fond Canonville	693,221	1,634,855	12.2	20.5	0.2	-	-	-
1167ZZ0040	Saint Pierre	Pecoul FR3	696,801	1,632,144	80.6	77.5	28.6	7.7E-02	3E-03	3rd ST. 2nd P.
1167ZZ0041	Saint Pierre	Pecoul	696,824	1,632,078	79.4	66	31.4	4.7E-03	3E-04	3rd ST. 2nd P.
1167ZZ0042	Saint Pierre	Pecoul FR1 bis	696,857	1,632,023	78.1	71.9	30.1	4.7E-03	2E-04	3rd ST. 2nd P.
1167ZZ0045	Saint Pierre	Piézomètre CDST	695,886	1,631,929	30.27	38.5	5.27	-	-	-
1167ZZ0058	Saint Pierre	Pecoul FR7	696,885	1,631,971	77	72	28	-	-	-

Table 2 (continued)

National number	City	Boreholes name or locality	X (m)	Y (m)	Borehole elevation (m)	Borehole depth (m)	Water level elevation (in m amsl)	T (m^2/s)	K (m/s)	Aquifer geology
1168ZZ0007	Ajoupa Bouillon	Saut Babin S1bis	704,056	1,638,469	158.4	35	-	-	-	-
1168ZZ0008	Ajoupa Bouillon	Fond Labour S4	704,386	1,638,009	161.6	50	-	-	-	-
1168ZZ0012	Ajoupa Bouillon	Ravine Bœuf S8	704,916	1,638,079	153.9	30	-	-	-	-
1168ZZ0013	Ajoupa Bouillon	L'école S9	705,366	1,639,269	169.6	45	-	-	-	-
1168ZZ0015	Ajoupa Bouillon	Dufailly S1	703,906	1,639,009	174.4	50	-	-	-	-
1168ZZ0016	Ajoupa Bouillon	Vivies S2	703,966	1,639,829	178.5	50	-	-	-	-
1168ZZ0017	Ajoupa Bouillon	Les ombrages S3	704,126	1,640,089	145.8	20	-	-	-	-
1168ZZ0018	Ajoupa Bouillon	Trou congo S4	704,631	1,640,499	66.3	10	-	-	-	-
1168ZZ0042	Ajoupa Bouillon	Grande Savane	703,326	1,638,649	241	45	212	-	-	-
1168ZZ0043	Basse Pointe	Morne Balai	700,846	1,639,949	420	61	403	9.0E-05	2E-06	3rd ST. 1st P.
1168ZZ0044	Ajoupa Bouillon	Grande Savane	703,319	1,638,599	241	46.5	211	3.0E-03	2E-04	3rd ST. 2nd P.
1168ZZ0045	Ajoupa Bouillon	Grande Savane	703,326	1,638,649	230	45	201	1.0E-03	6E-05	3rd ST. 2nd P.
1168ZZ0048	Basse Pointe	Démare	701,586	1,640,419	290	41	273	-	-	-
1168ZZ0054	Basse Pointe	Chez Lélène	704,241	1,640,671	84	28	81	-	-	-
1168ZZ0061	Ajoupa Bouillon	Savane Pascal	701,340	1,638,360	426	70	376	-	-	-
1168ZZ0062	Ajoupa Bouillon	Savane Pascal	701,076	1,638,480	440	70	386	-	-	-
1168ZZ0069	Ajoupa Bouillon	Fr2	700,165	1,637,602	614	74	562	-	-	-
1168ZZ0070	Ajoupa Bouillon	Fr3	700,349	1,637,637	592	70	535	-	-	-
BSS003GXLM	Grand Rivière	Beauséjour E1SD1b	697,168	1,644,504	177.69	25	-	-	-	-
BSS003GYRU	Grand Rivière	Beauséjour E2SD4	697,201	1,644,302	200.82	30	-	-	-	-
BSS003GYVQ	Grand Rivière	Beauséjour E3SP1	697,021	1,643,996	239.25	35	-	-	-	-
BSS003GZUG	Grand Rivière	Beauséjour E4SD10	696,763	1,643,861	240.89	25	-	-	-	-
BSS003HALY	Grand Rivière	Beauséjour E5SD13	697,019	1,643,667	273.48	25	-	-	-	-
BSS003HBXQ	Grand Rivière	Beauséjour E6SP2	697,091	1,643,355	301.48	35	-	-	-	-
BSS003HBYK	Grand Rivière	Beauséjour E7SP3	697,091	1,643,104	323.83	41	-	-	-	-

Appendix 2

Table 3 Freshwater springs database (WGS84 coordinate system)

National No.	City name	X (m)	Y (m)	Z (m)
BSS002NMEU	GRAND'RIVIERE	696,868	1,644,875	117
BSS002NMEV	GRAND'RIVIERE	696,425	1,644,771	95
BSS002NMEW	MACOUBA	697,327	1,643,256	308
BSS002NMEX	MACOUBA	697,410	1,644,310	121
BSS002NMEY	MACOUBA	697,391	1,644,243	130
BSS002NMFX	BASSE-POINTE	700,006	1,641,830	323
BSS002NMFY	BASSE-POINTE	702,186	1,642,920	133
BSS002NMFZ	MACOUBA	699,286	1,641,170	468
BSS002NMGA	MACOUBA	699,900	1,643,075	182
BSS002NMGB	MACOUBA	699,886	1,643,020	183
BSS002NMGC	MACOUBA	699,206	1,645,579	29
BSS002NMGD	BASSE-POINTE	702,599	1,644,706	8
BSS002NMGE	MACOUBA	700,499	1,644,830	70
BSS002NMGG	BASSE-POINTE	700,508	1,642,183	252
BSS002NMGH	BASSE-POINTE	703,606	1,643,699	56
BSS002NMGJ	BASSE-POINTE	705,842	1,642,545	13
BSS002NMGK	BASSE-POINTE	702,274	1,641,452	181
BSS002NMGL	BASSE-POINTE	701,866	1,642,373	154
BSS002NMGM	BASSE-POINTE	703,905	1,641,285	124
BSS002NMGN	BASSE-POINTE	702,592	1,641,441	180
BSS002NMGR	BASSE-POINTE	703,835	1,642,325	79
BSS002NMGS	BASSE-POINTE	703,643	1,641,552	137
BSS002NMGT	LORRAIN	705,962	1,641,365	37
BSS002NMGV	MACOUBA	698,237	1,642,492	368
BSS002NMGW	MACOUBA	699,467	1,645,187	87
BSS002NMGX	MACOUBA	700,287	1,644,296	108
BSS002NMGY	MACOUBA	699,345	1,641,899	325
BSS002NMGZ	MACOUBA	699,013	1,642,520	326
BSS002NMHA	MACOUBA	698,849	1,643,932	115
BSS002NMHB	MACOUBA	698,633	1,643,539	203
BSS002NMHC	BASSE-POINTE	705,368	1,642,936	14
BSS002NMHD	BASSE-POINTE	700,282	1,641,938	294
BSS002NMHE	BASSE-POINTE	702,252	1,642,764	127
BSS002NMHF	MACOUBA	698,849	1,643,650	163
BSS002NMHG	MACOUBA	698,830	1,642,811	206
BSS002NMHH	MACOUBA	699,461	1,645,374	75
BSS002NMHJ	MACOUBA	700,673	1,644,466	108
BSS002NMNJ	AJOUPA-BOUILLON	700,457	1,637,684	577
BSS002NMNK	AJOUPA-BOUILLON	701,218	1,637,271	471
BSS002NMNM	BASSE-POINTE	700186	1,639,570	516
BSS002NMNN	SAINT-PIERRE	699,613	1,635,940	509
BSS002NMNP	AJOUPA-BOUILLON	698,353	1,638,131	909
BSS002NMNQ	SAINT-PIERRE	698,132	1,637,694	942
BSS002NMNR	MORNE-ROUGE	699,413	1,633,735	319
BSS002NMNT	MORNE-ROUGE	700,518	1,636,384	516
BSS002NMNU	BASSE-POINTE	701,009	1,640,118	380
BSS002NMNW	MORNE-ROUGE	700,648	1,635,733	509
BSS002NMNX	AJOUPA-BOUILLON	701,797	1,637,786	338
BSS002NMNY	AJOUPA-BOUILLON	704,116	1,640,286	112
BSS002NMPH	BASSE-POINTE	701,579	1,640,429	283
BSS002NMPJ	AJOUPA-BOUILLON	701,871	1,637,816	357
BSS002NMPK	AJOUPA-BOUILLON	701,888	1,637,710	361
BSS002NMPL	AJOUPA-BOUILLON	703,123	1,638,689	243
BSS002NMPM	AJOUPA-BOUILLON	701,899	1,638,287	353
BSS002NMPN	BASSE-POINTE	701,373	1,640,649	284
BSS002NMPP	BASSE-POINTE	701,186	1,640,475	306
BSS002NMPQ	BASSE-POINTE	700,871	1,639,950	413
BSS002NMPR	BASSE-POINTE	700,145	1,639,714	463
BSS002NMPW	LORRAIN	705,210	1,640,645	62
BSS002NMPY	LORRAIN	706,501	1,640,487	89
BSS002NMPZ	LORRAIN	706,157	1,640,525	98
BSS002NMQA	LORRAIN	704,188	1,637,731	169
BSS002NMQB	LORRAIN	703,737	1,637,752	255
BSS002NMQC	LORRAIN	704,911	1,639,548	158
BSS002NMQD	LORRAIN	704,943	1,638,054	168
BSS002NMQE	LORRAIN	705,228	1,637,875	193
BSS002NMQF	LORRAIN	704,345	1,637,461	182
BSS002NMQN	MORNE-ROUGE	700,463	1,635,844	521
BSS002NMQP	MORNE-ROUGE	700,078	1,633,848	363
BSS002NMQU	MORNE-ROUGE	700,449	1,634,790	463
BSS002NMQV	MORNE-ROUGE	700,094	1,633,080	340
BSS002NMQW	MORNE-ROUGE	700,532	1,636,359	526
BSS002NMQX	MORNE-ROUGE	700,220	1,636,200	539
BSS002NMQY	MORNE-ROUGE	699,928	1,636,314	600
BSS002NMQZ	MORNE-ROUGE	700,705	1,636,525	524
BSS002NMRE	AJOUPA-BOUILLON	701,820	1,637,709	366
BSS002NMRF	BASSE-POINTE	704,173	1,640,755	98
BSS002NMRG	AJOUPA-BOUILLON	700,961	1,638,730	460
BSS004HMLQ	AJOUPA-BOUILLON	699,228	1,637,997	674
BSS004HMLR	AJOUPA-BOUILLON	699,283	1,638,068	668
BSS004HMLS	SAINT-PIERRE	696,413	1,637,834	889
BSS004HMLT	MORNE-ROUGE	699,864	1,635,313	445
BSS004HMLU	MORNE-ROUGE	700,391	1,634,530	424
BSS004HMLV	PRECHEUR	695,979	1,638,964	600
BSS004HMLW	PRECHEUR	696,536	1,638,484	895
BSS004HMLX	MORNE-ROUGE	700,551	1,636,441	519
BSS004HMLZ	AJOUPA-BOUILLON	701,039	1,637,100	419
BSS004HMMA	AJOUPA-BOUILLON	701,052	1,637,111	419
BSS004HMMB	AJOUPA-BOUILLON	701,916	1,638,324	351
BSS004HMMC	AJOUPA-BOUILLON	704,090	1,640,130	132
BSS004HMMD	SAINT-PIERRE	699,182	1,636,330	563
BSS004HMME	BASSE-POINTE	699,089	1,639,074	677
BSS004HMMF	MACOUBA	697,749	1,639,784	689
BSS004HMMG	BASSE-POINTE	698,511	1,639,771	723
BSS002NMGQ	BASSE-POINTE	703,986	1,642,363	92
BSS002NMGP	BASSE-POINTE	703950	1,642,446	84

Appendix 3

Table 4 Thermal springs database (WGS84 coordinate system)

X (m)	Y (m)	Z (m)	Group Name
696,319	1,637,000	541	Chaude River springs
696,399	1,637,060	583	Chaude River springs
696,462	1,637,050	604	Chaude River springs
696,511	1,637,050	604	Chaude River springs
696,308	1,637,660	768	Claire River springs
696,284	1,637,660	768	Claire River springs
696,306	1,637,680	784	Claire River springs
696,154	1,637,530	727	Claire River springs
696,191	1,637,560	730	Claire River springs
696,001	1,637,320	648	Claire River springs
695,954	1,637,130	576	Claire River springs
694,163	1,636,700	233	Mitan and Picodo springs
694,027	1,636,650	219	Mitan and Picodo springs
693,663	1,636,750	222	Mitan and Picodo springs
693,523	1,636,510	158	Mitan and Picodo springs
694,021	1,633,250	0	Underwater springs
693,717	1,633,800	0	Underwater springs
693,832	1,633,470	0	Underwater springs
693,766	1,633,680	0	Underwater springs
693,644	1,633,910	0	Underwater springs
695,233	1,632,340	0	Underwater degassing zone
695,283	1,632,270	0	Underwater degassing zone
695,376	1,632,140	0	Underwater degassing zone
695,386	1,632,080	0	Underwater degassing zone
695,408	1,632,020	0	Underwater degassing zone
695,433	1,631,990	0	Underwater degassing zone
697,140	1,639,530	865	Grande Rivière spring
698,039	1,637,220	790	Des Pères River springs
698,132	1,637,180	753	Des Pères River springs

Supplementary Information The online version contains supplementary material available at https://doi.org/10.1007/s10040-023-02642-5.

Declarations Conflict of interest On behalf of all authors, the corresponding author states that there is no conflict of interest.

References

Aldous A, Gurrieri J (2011) Environmental flows and levels for groundwater-dependent fens of the antelope grazing allotment, Fremont-Winema National Forest, Oregon. The Nature Conservancy, Arlington, VA

Arnaud L, Leclerc B (2010) Forages 1165ZZ0012/F4 et 1165ZZ0013/F5: travaux et pompages d'essais, commune de Grand-Rivière [Boreholes 1165ZZ0012/F4 and 1165ZZ0013/F5: drilling and pumping tests results, municipality of Grand-Rivière]. BRGM open file report RP-58633-FR, BRGM, Orléans, France

Arnaud L, Lanini S (2014) Impact du changement climatique sur les ressources en eau de Martinique [Impact of climate change on Martinique water ressources]. Rapport BRGM/RP-62676-FR, pp 91

Auken E, Christiansen AV, Westergaard JH, Kirkegaard C, Foged N, Viezzoli A (2009) An integrated processing scheme for high-resolution airborne electromagnetic surveys, the SkyTEM system. Explor Geophys 40:184–192

Barat A (1986) Étude du rôle des eaux souterraines dans le mécanisme des éruptions phréatiques. Application à la Montagne Pelée de Martinique et à la Soufrière de Guadeloupe [Study of the role of groundwater in the mechanism of phreatic eruptions: application to the Montagne Pelée of Martinique and the Soufrière of Guadeloupe]. BRGM report no. 115, BRGM, Orléans, France, 205 pp

Bogie I, Mackenzie K (1998) The application of a volcanic facies model to an andesitic stratovolcano hosted geothermal system at Wayang Windu, Java, Indonesia. In: Proceedings 20th NZ Geothermal Workshop, Aukland, 1998, pp 265–270

Boudon G, Balcone-Boissard H (2021) Volcanological evolution of Montagne Pelée (Martinique): a textbook case of alternating plinian and dome-forming eruptions, earth-science reviews, volume 221. https://doi.org/10.1016/j.earscirev.2021.103754

Boudon G, Le Friant A, Komorowski JC, Deplus C, Semet MP (2007) Volcano flank instability in the Lesser Antilles arc: diversity of scale, processes, and temporal recurrence. J Geophys Res: Solid Earth 112(B8)

Brown SK, Jenkins SF, Sparks RSJ, Odbert H, Auker MR (2017) Volcanic fatalities database: analysis of volcanic threat with distance and victim classification. J Appl Volcanol 6:15. https://doi.org/10.1186/s13617-017-0067-4

Cabrera MC, Custodio E (2019) Conceptual hydrogeological models of oceanic intraplate volcanic small. Islands proceedings of IAH2019, the 46th annual congress of the International Association of Hydrogeologists, Málaga, Spain, 22–27 September 2019

Custodio E (1975) Hydrogeologia de las rocas volcanicas [Hydrogeology of volcanic rocks]. 3rd UNESCO-ESA-IHA symposium on groundwater, UNESCO, Paris, pp 23–69

Custodio E, Lopez Garcia L, Amigo E (1988) Simulation par modèle mathématique de l'île volcanique de Ténériffe (Canaries, Espagne) [Mathematical model simulation of the volcanic island of Tenerife (Canary Islands, Spain)]. Hydrogéologie 1988(2):153–167

Deparis J, Reninger PA, Perrin J, Martelet G, Audru JC (2014) Acquisition géophysique héliportée de la Martinique [Helicopter-borne geophysical acquisition of Martinique]. Open file BRGM Report RP-62428-FR. http://infoterre.brgm.fr/rapports/RP-62428-FR.pdf. Accessed May 2023

Dumont M, Peltier A, Roblin E, Reninger PA, Barde-Cabusson S, Fininzola A, Ferrazzini V (2019) Imagery of internal structure and destabilization features of active volcano by 3D high resolution airborne electromagnetism. Sci Rep 9:18280. https://doi.org/10.1038/s41598-019-54415-4

Domenico PA, Schwartz FW (1990) Physical and chemical hydrogeology. Wiley, New York, 824 pp

d'Ozouville N, Auken E, Sorensen KI, Violette S, de Marsily G (2008) Extensive perched aquifer and structural implications

revealed by 3D resistivity mapping in a Galapagos volcano. Earth Planet Sci Lett 269:517–521

Fabre R, Chaigneau M (1960) Technique de prélèvement et d'analyse de gaz de fumerolles de volcans. Exemple d'analyses de gaz prélevés à la montagne Pelée (Martinique) et à la Grande Soufrière (Guadeloupe) [Technique of sampling and analysis of fumarole gases from volcanoes: example of gas analysis from mount Pelee (Martinique) and Grande Soufrière (Guadeloupe)]. Bull Volcanol 23:21–30. https://doi.org/10.1007/BF02596625

Fontaine FR, Corbeau J, Vaton D, the OVSM-IPGP team (2022) Rapport d'activité 2021 de l'Observatoire Volcanologique et Sismologique de Martinique [Activity report 2021 of the Volcanological and Seismological Observatory of Martinique). Institut de Physique du Globe de Paris, Paris

Gadalia A, Baltassat JM, Bouchot V, Caritg S, Coppo N, Gal F, Girard JF, Gutierrez A, Jacob T, Martelet G, Rad S, Tailame AL, Traineau H, Vittecoq B, Wawrzyniak P, Zammit C (2014) Compléments d'exploration géothermique en Martinique: conclusions et recommandations pour les zones de la Montagne Pelée, des Anses d'Arlet, des Pitons du Carbet et du Lamentin [Complementary geothermal exploration in Martinique: conclusions and recommendations for the Montagne Pelée, Anses d'Arlet, Pitons du Carbet and Lamentin areas]. BRGM report RP- 63019-FR, BRGM, Orléans, France

Germa A, Quidelleur X, Labanieh S, Lahitte P, Chauvel C (2010) The eruptive history of Morne Jacob volcano (Martinique Island, French West Indies): geochronology, geomorphology and geochemistry of the earliest volcanism in the recent Lesser Antilles Arc. J Volcanol Geotherm Res 198:297–310

Germa A, Quidelleur X, Labanieh S, Chauvel C, Lahitte P (2011a) The volcanic evolution of Martinique Island: insights from K–Ar dating into the Lesser Antilles arc migration since the Oligocene. J Volcanol Geotherm Res 208(2011):122–135

Germa A, Quidelleur X, Lahitte P, Labanieh S, Chauvel C (2011b) The K-Ar Cassignol-Gillot technique applied to Western Martinique lavas: a record of Lesser Antilles arc activity from 2 ma to Mount Pelée volcanism. Quat Geochronol 6:341–355. https://doi.org/10.1016/j.quageo.2011.02.001

Guiscafre J, Klein JC, Moniod F (1976) Les ressources en eau de surface de la Martinique [The surface water resources of Martinique]. Monographies hydrologiques ORSTOM, Noumea, France

Hemmings B, Whitaker F, Gottsmann J, Hughes A (2015) Hydrogeology of Montserrat, review and new insights. J Hydrol Reg Stud 3:1–30. https://doi.org/10.1016/j.ejrh.2014.08.008

Lacroix A (1904) La Montagne Pelée et ses eruptions [Mount Pelee and its eruptions]. Masson, Paris, 662 pp

Le Friant A, Boudon G, Deplus C, Villemant B (2003) Large scale flank-collapse during the recent activity of Montagne Pelee, Martinique. J Geophys Res 108(B1):2055

Legendre Y (2012) Reconstruction fine de l'histoire éruptive et scenarii éruptifs à la soufrière de Guadeloupe: vers un modèle intégré de fonctionnement du volcan [Fine reconstruction of the eruptive history and eruptive scenarios at the Guadeloupe Soufrière: towards an integrated model of the volcano]. Thèse, Université Paris Cité, 675 pp

Lipman PW, Mullineaux DR (1981) The 1980 eruptions of Mount St. Helens. US Geol Surv Prof Pap 1250, 844 pp. https://pubs.usgs.gov/pp/1250/report.pdf. Accessed May 2023

Macdonald GA, Abbott AT, Peterson FL (1983) Volcanoes in the sea: the geology of Hawaii. University of Hawaii Press, Honolulu, 571 pp

Meinzer OE (1930) Ground water in the Hawaiian Islands, in geology and water resources of the Kau District, Hawaii. US Geol Surv Prof Pap 616:1–28

Michaud-Dubuy A (2019) Dynamique des eruptions Pliniennes: réévaluation de L'aléa Volcanique en Martinique [Dynamics of Plinian eruptions: reassessment of the volcanic Hazard in Martinique]. Thèse, Université de Paris, Paris, 200 pp

Peruzzetto M, Legendre Y, Nachbaur A, Dewez TJB, Thiery Y, Levy C, Vittecoq B (2022) How volcanic stratigraphy constrains headscarp collapse scenarios: the Samperre Cliff case study (Martinique island, Lesser Antilles). Nat Hazards Earth Syst Sci 22:3973–3992. https://doi.org/10.5194/nhess-22-3973-2022

Peterson FL (1972) Water development on tropic volcanic islands: type example—Hawaii. Ground Water 10(5):18–23

Pyle DM, Barclay J, Armijos MT (2018) The 1902–3 eruptions of the Soufrière, St Vincent: impacts, relief and response. J Volcanol Geothermal Res 356:183–199. https://doi.org/10.1016/j.jvolgeores.2018.03.005

Pryet A (2011) Hydrogeology of volcanic islands: a case-study in the Galapagos archipelago (Ecuador). PhD Thesis, Université Paris 6 Pierre et Marie Curie, Paris

Pryet A, Ramm J, Chiles JP, Auken E, Deffontaines B, Violette S (2011) 3D resistivity gridding of large AEM datasets: a step toward enhanced geological interpretation. J Appl Geophys 75:277–283

Pryet A, D'ozouville N, Violette S, Deffontaines B, Auken E (2012) Hydrogeological settings of a volcanic island (San Cristobal, Galapagos) from joint interpretation of airborne electromagnetics and geomorphological observations. Hydrol Earth Syst Sci 16(12):4571–4579

Rad S, Rivé K, Vittecoq B, Cerdan O, Allègre JC (2013) Chemical weathering and erosion rates in the Lesser Antilles: an overview in Guadeloupe, Martinique and Dominica. J South Am Earth Sci 45:331–344. https://doi.org/10.1016/j.jsames.2013.03.004

Reninger PA, Martelet G, Deparis J, Perrin J, Chen Y (2011) Singular value decomposition as a denoising tool for airborne time domain electromagnetic data. J Appl Geophys 75:264–276. https://doi.org/10.1016/j.jappgeo.2011.06.034

Reninger PA, Martelet G, Perrin J, Dumont M (2020) Processing methodology for regional AEM surveys and local implications. Explor Geophys 51(1):143–154. https://doi.org/10.1080/08123985.2019.1680249

Robertson REA (1995) An assessment of the risk from future eruptions of the Soufrière volcano of St Vincent, West Indies. Nat Hazards 11:163–191

Robins NS, Lawrence AR, Cripps AC (1990) Problems of groundwater development in small volcanic islands in the eastern Caribbean. In: Krishna JH, Quiñones-Aponte V, Gómez-Gómez F, Morris G (eds) Tropical hydrology and Caribbean water resources. American Water Resources Association, Bethesda, MD, pp 257–267

Rosas-Carbajal M, Komorowski JC, Nicollin F, Gibert D (2016) Volcano electrical tomography unveils edifice collapse hazard linked to hydrothermal system structure and dynamics. Sci Rep 6:29899. https://doi.org/10.1038/srep29899

Selles A (2014) Multidisciplinary study about the hydrogeological behavior of the eastern flank of Merapi volcano, Central Java, Indonesia. PhD Thesis, Université Paris 6 Pierre et Marie Curie, Paris

Selles A, Deffontaines B, Hendrayana H, Violette S (2015) The eastern flank of the Merapi volcano (Central Java, Indonesia): architecture and implications of volcaniclastic deposits. J Asian Earth Sci 108(2015):33–47

Sørensen KI, Auken E (2004) SkyTEM: a new high-resolution helicopter transient electromagnetic system. Explor Geophys 35:191–199

Spies BR (1989) Depth of investigation in electromagnetic sounding methods. Geophysics 54:872–888. https://doi.org/10.1190/1.1442716

Taïlamé AL, Lanini SS (2020) – Définition des volumes prélevables en Martinique. Rapport final [Definition of withdrawable water volumes in Martinique. Final Report]. BRGM/RP-68883-FR, pp 49

Traineau H, Westercamp D, Benderitter Y (1989) Case study of a volcanic geothermal system, Mount Pelée, Martinique. J Volcanol Geotherm Res 38:49–66

Vessell RK, Davies DK (1981) Nonmarine sedimentation in an active fore arc basin. In: Recent and ancient nonmarine depositional environments: models for exploration: Society of Economic Paleon Tologists and Mineralogists Special Paper 31. SEPM Society for Sedimentary Geology, Broken Arrow, OK, pp 31–45. https://doi.org/10.2110/pec.81.31.0031

Viezzoli A, Christiansen AV, Auken E, Sørensen K (2008) Quasi-3D modeling of airborne TEM data by spatially constrained inversion. Geophysics 73:F105–F113

Villemant B, Le Friant A, Caron B, Del Manzo G, Lafuerza S, Emmanuel L, Ishizuka O, Guyard H, Labourdette N, Hidalgo MA (2022) A 1.5 ma marine record of volcanic activity and associated landslides offshore Martinique (Lesser Antilles): sites U1397 and U1399 of IODP 340 expedition. Front Earth Sci 10:767485. https://doi.org/10.3389/feart.2022.767485

Vincent PM, Bourdier JL, Boudon G (1989) The primitive volcano of Montagne Pelee: its construction and partial destruction by flank collapse. In: Boudon G, Gourgaud A (eds) Montagne Pelée. J Volcanol Geotherm Res 38:1–15

Violette S, d'Ozouville N, Pryet A, Deffontaines B, Fortin J, Adelinet M (2014) Hydrogeology of the Galapagos archipelago: an integrated and comparative approach between islands. In: Harpp KS, Mittelstaedt EL, D'Ozouville N, Graham DW (eds) The Galápagos as a laboratory for the earth sciences, vol 9. American Geophysical Union, Washington, DC, pp 167–183

Vittecoq B, Lachassagne P, Lanini S, Ladouche B, Marechal JC, Petit V (2007) Elaboration d'un système d'information sur les eaux souterraines de la Martinique: identification et caractérisations quantitatives [elaboration of an information system on groundwater in Martinique: identification and quantitative characterizations]. Open file BRGM report RP-55099-FR. http://infoterre.brgm.fr/rapports/RP-55099-FR.pdf. Accessed May 2023

Vittecoq B, Lachassagne P, Lanini S, Maréchal JC (2010) Evaluation des ressources en eau de la Martinique : calcul spatialisé de la pluie efficace et validation à l'échelle du bassin-versant [Evaluation of water resources in Martinique: spatialized calculation of effective rainfall and validation at the watershed scale]. Rev Sci Eau 23(4):361–373

Vittecoq B, Deparis J, Violette S, Jaouen T, Lacquement F (2014) Influence of successive phases of volcanic construction and erosion on Mayotte Island's hydrogeological functioning as determined from a helicopter-borne resistivity survey correlated with borehole geological and permeability data. J Hydrol 509:519–538. https://doi.org/10.1016/j.jhydrol.2013.11.062

Vittecoq B, Reninger PA, Violette S, Martele G, Dewandel B, Audru JC (2015) Heterogeneity of hydrodynamic properties and groundwater circulation of a coastal andesitic volcanic aquifer controlled by tectonic induced faults and rock fracturing: Martinique Island (Lesser Antilles - FWI). J Hydrol 529:1041–1059. https://doi.org/10.1016/j.jhydrol.2015.09.022

Vittecoq B, Reninger PA, Lacquement F, Martelet G, Violette S (2019) Hydrogeological conceptual model of andesitic watersheds revealed by high-resolution heliborne geophysics. Hydrol Earth Syst Sci 23:2321. https://doi.org/10.5194/hess-23-2321-2019

Wadge G, Voight B, Sparks RSJ, Cole PD, Loughlin SC, Robertson REA (2014) An overview of the eruption of Soufrière Hills volcano, Montserrat from 2000 to 2010. Memoir 39, Geological Society, London, 40 pp

Ward SH, Hohmann GW (1988) Electromagnetic theory for geophysical applications: electromagnetic methods. Appl Geophys 1:130–311

Westercamp D, Traineau H (1983) - Carte géologique de la Montagne Pelée à 1/20 000 (département de la Martinique) et notice explicative simplifiée [Montagne Pelée 1/20 000 geological map (Martinique) with simplified notice]. Éd. BRGM

Westercamp D, Andreieff P, Bouysse P, Cottez S, Battistini R (1989) Notice explicative, carte géol. France (1/50 000), feuille Martinique (explanatory note, Geol. Map France (1/50 000), sheet Martinique. BRGM, Orléans, France, 246 pp

Westercamp D, Pelletier B, Thibaut PM, Traineau H, Andreieff P (1990) Carte géologique de la France (1/50.000), feuille Martinique [Geological map of France (1/50,000), Martinique sheet]. BRGM, Orléans, France. http://infoterre.brgm.fr/. Accessed May 2023

Zlotnicki J, Boudon G, Viodé JP, Delarue JF, Mille A, Bruère F (1998) Hydrothermal circulations beneath Montagne Pelée inferred by self-potential surveying: structural and tectonic implications. J Volcanol Geotherm Res 84:73–91